Thesis for the degree of doctor of medicine

Measurements of the DNA double-strand break response

Aida Muslimović

UNIVERSITY OF GOTHENBURG

Department of Clinical Chemistry and Transfusion Medicine
Institute of Biomedicine
Sahlgrenska Academy
University of Gothenburg
2012

Cover illustration: Cell nuclei with P-H2AX foci labeled with fluorescent antibodies.

Printed by Ineko AB, Gothenburg, Sweden

aida.muslimovic@gu.se

ISBN 978-91-628-8504-5

To my parents

ABSTRACT

Radiotherapy and some chemotherapeutic drugs kill cancer cells by induction of the extremely toxic DNA double-strand breaks (DSBs). Measurements of the DSB response in patients during therapy could allow personalized dosing to improve tumor response and minimize side effects. DSBs induce a strong cellular response via phosphorylation of H2AX, P-H2AX and the formation of foci. P-H2AX can be measured by flow cytometry or counted in separate cell nuclei by immunofluorescence microscopy. The overall aim of my research has been to develop and validate methods to measure P-H2AX in mononuclear cells from cancer patients undergoing radiotherapy.

Initially, we wanted to characterize DNA damage induced by the chemotherapeutic drug etoposide that induces TopoII-linked DSBs and to test its ability to activate the P-H2AX response using a flow cytometry-based P-H2AX assay. We found that only 0.3% of etoposide-induced DSBs activated the H2AX response and toxicity. We concluded that the P-H2AX response was a good measure of the toxic effects of etoposide.

Next, we wanted to optimize the flow cytometry assay for mononuclear cells from cancer patients undergoing radiation therapy. The P-H2AX response was measured before and after 5Gy pelvic irradiation and in *in vitro*-irradiated controls. We found a fraction of cells with high P-H2AX signals that corresponded to the 5Gy *in vitro*-irradiated blood controls. This study indicated that flow cytometry may be well suited for measurements of the P-H2AX response in mononuclear cells following local radiotherapy.

To be able to implement the P-H2AX assay in clinical practice and use it in relation to clinical outcome and side effects we have also developed stable and reliable calibrators based on phosphopeptide-coated beads and fixed cells. Using these calibrators it could be possible to use the P-H2AX flow cytometry assay in the clinic in a controlled manner.

Finally, using immunostaining in solution before cells are mounted on microscopic slides for quantification of single P-H2AX foci by immunofluorescence, we have the possibility to analyze 16 patient samples within few hours, which makes this method suitable for clinical use.

Keywords: *DNA double-strand break, DSB; phosphorylated H2AX, P-H2AX; etoposide; ionizing radiation, IR; flow cytometry; calibrators; immunofluorescence; P-H2AX foci.*

ISBN: 978-91-628-8504-5

LIST OF PAPERS

This thesis is based on the following studies, referred to in the text by their Roman numerals.

I. Muslimović A, Nyström S, Gao Y, Hammarsten O. Numerical analysis of etoposide induced DNA breaks. PLoS ONE 2009 4(6):e5859.

II. Muslimović A, Ismail IH, Gao Y, Hammarsten O. An optimized method for measurement of gamma-H2AX in blood mononuclear and cultured cells. Nat Protocols 2008 3(7):1187-93.

III. Muslimović A, Johansson P, Ruetschi U, Hammarsten O. Calibrators for clinical measurements of phosphorylated H2AX in patient cells by flow cytometry. Submitted Manuscript.

IV. Johansson P, Muslimović A, Hultborn R, Fernström E, Hammarsten O. In-solution staining and arraying method from the immunofluorescence detection of γH2AX foci optimized for clinical applications. Biotechniques 2011 51(3):185-9.

CONTENT

ABBREVIATIONS

DNA	Deoxyribonucleic acid
EC	Euchromatin
HC	Heterochromatin
ROS	Reactive oxygen species
AP sites	Abasic/apyriminic/apuric sites
IR	Ionizing radiation
SSBs	Single-strand DNA breaks
DSBs	Double-strand DNA breaks
NHEJ	Non-homologous end joining
HR	Homologous recombination
CSR	Class switch recombination
LET	Linear energy transfer
CLM	Calicheamicin γ-1
TopoII	Topoisomerase II
RNA	Ribonucleic acid
SOD	Superoxide dismutase
BER	Base excision repair
NER	Nucleotide excision repair
DNA-PK	DNA-dependent protein kinase

PNK	Polynucleotide kinase
APLF	Aprataxin and PNK-like factor
XRCC4	X-ray cross-complementing 4
XLF/Cernunnos	XRCC4-like factor
LigIV	DNA Ligase IV
Ku	Ku70/80 heterodimer
RAG1	Recombination activating gene 1
RAG2	Recombination activating gene 2
CtIP	C-Terminal Binding Protein Interacting Protein
PARP1	Poly [ADP-ribose] polymerase 1
LigIII	DNA-ligase III
XRCC1	X-ray repair cross-complementing 1
TBH	Tert-butyl hydroperoxide
ATM	Ataxia telangiectasia mutated
H2AX	Histone 2 variant H2A.X
P-H2AX	Gamma-H2AX
MRN	Mre11-Rad50-Nbs1/Nibrin complex
MDC1	Mediator of DNA damage checkpoint protein 1
RNF8	Ring finger protein 8
RNF168	Ring finger protein 168
53BP1	p53 binding protein 1
KAP1	(Krüppel-associated box)-zinc finger protein-associated protein 1

CHD3	Chromodomain-helicase-DNA-binding protein 3
SUMO1	Small ubiquitin-related modifier 1
ATR	Ataxia telangiectasia and Rad-3-related
PIKKs	Phosphatidylinositol-OH-kinase-like family of protein kinases
ATRIP	ATR interacting protein
ssDNA	Single-stranded DNA regions
RPA	Replication protein A
Chk1	Checkpoint kinase 1
Chk2	Checkpoint kinase 2
p53	Tumor protein 53
Nbs1	Nibrin
TopBP1	Topoisomerase II β-binding protein
WSTF	Williams-Beuren syndrome transcription factor
MAPK8/JNK1	Mitogen-activated kinase 8
EYA	Eyes absent
HATs	Acetyltransferases
HDACs	Histone deacetylases
Tip60	Tat-interacting protein 60
Ubc13	Ubiquitin conjugating enzyme 13
BRCA1	Breast cancer type 1 susceptibility protein
HERC2	HECT and RLD domain containing E3 ubiquitin protein ligase 2
UIM	Ubiquitin interacting motif

Rap80	Receptor associated protein 80
SUMO	Small ubiquitin-like modifier
PP	Protein phosphatase
WIP1	Wild-type-53-induced phosphatase
A-T	Ataxia telangiectasia
ATLD	Ataxia telangiectasia-like disorder
SCID	SCID
CT	Computerized tomography
DLP	Dose-length product
Gy	Gray (J/kg)
MRT	Magnetic resonance tomography
CFGE	Constant field gel electrophoresis

1 INTRODUCTION

1.1 DNA and chromatin

A copy of our genetic information is kept well preserved in the cell nuclei of each cell in our body. The genetic information is encoded by two-meter long polymeric molecules called deoxyribonucleic acid (DNA) that guide most processes in the cell.DNA is built up of nucleotides containing a phosphate group, a sugar group (2-deoxyribose) and a base attached to each sugar. The nucleotides are connected to each other by phosphodiester bonds between sugar groups creating long DNA strands with the bases placed in a specific manner. Two DNA strands are linked together by strong hydrogen bonds between bases: adenine-thymine and guanine-cytosine, creating a double-helix. Each DNA strand acts as a template for a new complementary strand in the replication process that passes on genetic information from generation to generation and essentially is the driving force behind continued life on earth [1].

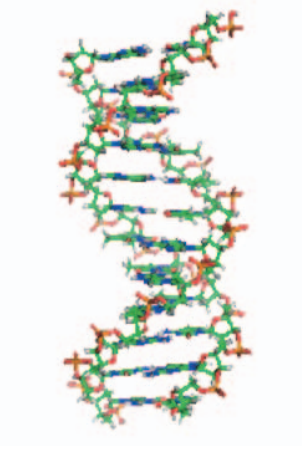

Figure 1. The structure of DNA, adapted from Ola Hammarsten.

The DNA of our cells is organized in DNA-protein complexes called chromatin. Chromatin proteins mostly consist of histones, small arginine-lysine-rich proteins with high binding affinity for the negatively charged DNA. Chromatin is organized in smaller structural subunits called nucleosomes. The bead particles called nucleosome core particles contain about 150bp of DNA coiled 1.7 times around the core consisting of eight histones, two from each of the H2A, H2B, H3 and H4 types, and an additional 50bp of DNA for the linker-histone H1 connecting two nucleosomes. The nucleosome structure results in a packaging of DNA into 10nm fibers, which can be further compressed into 30nm fibers and chromosomes. The human genome is made up of 46 chromosomes [2].

There are two forms of chromatin, the compactly packed form heterochromatin (HC) and the lightly packed euchromatin (EC), which presents the active form of the genome; i.e., active gene transcription. Heterochromatin (HC) makes up 10-25% of all chromatin depending on age, cell type and species. HC can be divided into two forms: constitutive HC, which contains transcriptionally inert DNA remaining silent throughout life like centromeres and telomeres, and facultative HC that includes genes originally comprised within transcriptionally active EC, but silenced during development or aging [3].

1.2 DNA damage and repair

Our DNA is constantly subjected to DNA damage. Approximately 10 000 DNA lesions are induced in each cell every day, corresponding to approximately 10^{17} DNA lesions per person per day [2]. The majority of these lesions are caused by spontaneous reactions with water or by reactive oxygen species (ROS) produced during a normal aerobic metabolism, replication errors generated during DNA synthesis, but also by exogenous factors such as ionizing radiation and chemicals [2]. Unrepaired or misrepaired DNA damage can lead to chromosomal rearrangements and translocations and consequently cancer and cell death. In order to survive, our cells have developed multiple sophisticated DNA repair systems to repair various forms of DNA damage.

1.2.1 DNA damage

Depending on the source, different types of DNA damage is induced. Simply due to the aqueous environment around the DNA, bases can be lost by breakage of the N-glycosidic bond between deoxyribose and bases creating abasic/apyriminic/apuric sites (AP sites). Bases can also be deaminated and, for instance, convert cytosine to uracil, which will eventually cause mutations. ROS leaking from the respiratory chain in the mitochondria can cause highly mutagenic lesions like 8-oxo-guanine. Sunlight (UV radiation) can induce pyrimidine dimers that, if not repaired, may mis-pair during

replication and also result in mutations. Ionizing radiation (IR), on the other hand, can, beside base damage, also generate breaks in the DNA backbone causing single-strand DNA breaks (SSBs) and double-strand DNA breaks (DSBs) [2].

1.2.2 DNA double-strand breaks (DSBs)

One of the most toxic DNA lesions is the DNA double-strand break (DSB). A DSB is formed when the phosphodiester bond between the sugars on both DNA strands is broken and if this occurs with a distance of 10-20 base pairs on the opposing DNA strands [4]. Only 1-10 DSBs can induce p53-dependent G1 arrest and cell death [5]. For this reason, DSBs are extremely toxic and used in cancer treatment to kill tumor cells.

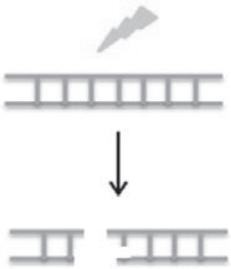

Figure 2. DNA double-strand break.

Single-stranded DNA damage, on the other hand, is removed with a half-life of minutes, as there is an intact DNA copy to guide the repair. Single-stranded DNA damage is therefore not very toxic and in some instances over 100 000 SSBs are required to induce cell-cycle arrest. DSBs cannot be repaired by template-directed repair systems, as both DNA strands are broken. DNA ends in a DSB can either be directly rejoined by a process that requires little or no homology, called non-homologous end joining (NHEJ), or repaired by homologous recombination (HR) that uses an undamaged sister chromatid as the template for repair.

DSBs can be induced by IR and many chemotherapeutic drugs like bleomycin and etoposide. DSBs can also be generated as a consequence of normal cellular processes like oxidative respiration that generates ROS, stalled replication forks, meiotic recombination, V(D)J recombination, class switch recombination (CSR), and at eroded telomeres.

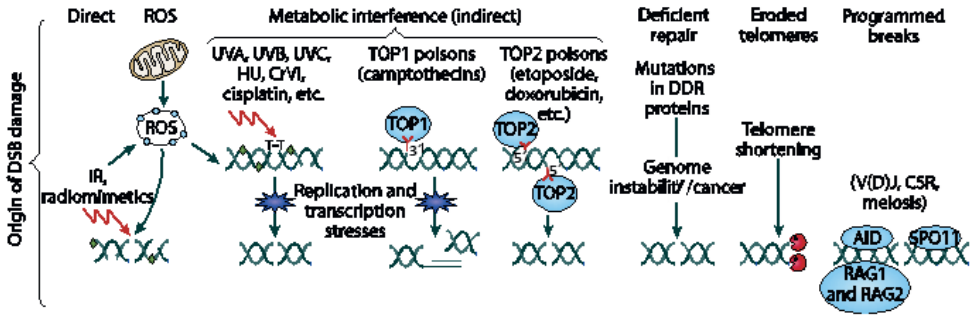

Figure 3. Different origins of DSBs. Adapted with permission from Nature reviews cancer; "γ-H2AX and cancer", Bonner, W.M. et al, p.959.

1.2.3 Endogenous DSBs

V(D)J recombination

V(D)J recombination is a site-specific recombination process involving induction of DSBs that are repaired by NHEJ (non-homologous end joining). V(D)J is necessary for the development of the immune system and its high diversity. B and T lymphocytes are two major cell types involved in the immune response. B lymphocytes fight foreign substances by secretion of antibodies that react with soluble antigens, while T lymphocytes express T cell receptors that react with antigens expressed on the surface of cells. Antibodies are composed of two heavy and two light polypeptide chains. Each polypeptide chain is composed of a C terminal constant region and a N terminal variable region. The diversity of the variable regions is generated by V(D)J recombination that recombines several different alternative gene segments into one continuous exon that encodes the variable N-terminal

region of the light and heavy chains. T cell receptors also contain variable and constant regions in their α and β chains that also are assembled by V(D)J recombination.

The diversity of the variable regions is generated at several levels. First, there are multiple copies of the gene regions V (variable), D (diverse) and J (joining) that can be recombined in multiple ways, in the heavy chain. In a similar manner, the variable regions in the light chains are built by recombination of V, J regions. Second, as the V(D)J recombination independently generates variable regions in the heavy and the light chain in each B-cell, the combination of different heavy and light chains into one antibody result in high diversity. In addition, NHEJ, the process that joins together cleaved coding regions during V(D)J recombination, is error-prone, leading to deletions and insertions of nucleotides, further amplifying the diversity of the antigen binding region of the antibodies.

V(D)J recombination is initiated by Rag1 and Rag2 (recombination activating genes 1 and 2) that induce a DSB between the RSS sequence (recombination-specific sequence) and the coding sequence of a gene segment. Coding ends are generated as hairpin intermediates that must be opened before they can be joined. The hairpins are opened by the nuclease Artemis that acquires its endonuclease activity after interaction and phosphorylation by DNA-PKcs [6]. The intervening DNA-segment that is cleaved out from the genome by RAG1/RAG2, the non-coding regions, expose blunt double-stranded DNA ends. Both the opened coding ends and the non-coding ends are joined by NHEJ[7].

Class-switch recombination (CSR)

Other immune processes coupled to DSB generation are CSR and somatic hypermutation, responsible for the maturation of B lymphocytes. CSR transfers a rearranged variable region to a constant region anywhere within the switch regions. A key player in both processes is AID (activation-induced deaminase) that locally deaminates cytosine in DNA to urasil (C-U) [8]. Removal of uracil by base excision repair results in SSBs. Since switch regions are rich in C-G pairs, the multiple deaminations that are induced locally around the switch-regions will result in the formation of DSBs that enable class-switch recombination. Somatic hypermutation within the variable regions is believed to occur from a high frequency of errors during the repair of C-U deaminations.

Meiotic recombination

The recombination of homologous chromosomes after DNA replication in meiosis is initiated by DSBs induced by the endonuclease Spo11. Spo11 acts

as a type II topoisomerase and generates protein-linked DSBs. A Spo11 dimer cleaves both DNA strands in a coordinated manner, creating a DSB with covalent linkages between the newly created 5´-DNA ends and the catalytic tyrosine residue in Spo11. Spo11 is removed by endonucleolytic cleavage uncovering DSBs that are resected to 3´-ssDNA. Rad51 binds together with meiosis-specific recombinase Dmc1 and generates the nucleoprotein filaments required for the homology search in the homologous chromosome [9, 10].

1.2.4 Ionizing radiation-induced DNA damage

Ionizing photons or particles (ionizing radiation (IR)) induce DNA damage in two ways. By direct energy deposition to DNA, leading to a single ionization event within the DNA molecule, as well as indirectly by ionization of water molecules generating multiple hydroxyl radicals and clustered DNA damage within a few base pairs [11]. DNA damage induced by IR can contain oxidized bases, AP sites, sugar lesions, heat or alkaline labile sites, crosslinks (DNA protein or DNA-DNA covalent bindings), SSBs and DSBs [12].

Photons and electrons are most commonly used in radiation treatment. Photons can be generated from radioactive isotopes or by Röntgen/X-ray radiation or accelerators. The photon transfers a part of its energy to an electron in an atom it encounters. The electron subsequently leaves the atom and ionizes other atoms by energy transfer to their electrons. In electron radiation the electrons are ionizing atoms directly within the ionization track [11, 13].

The passing photon or particle induces multiple ionizations as it passes through biological tissue; however, it can be sparsely or densely distributed depending on the particles used. Photons, electrons and protons generate lower ionization densities (low linear energy transfer, low LET) with larger distances between the ionization events than neutrons while α particles produce multiple ionizations in a dense area (high linear energy transfer, high LET). The higher the density of the particles and, consequently, ionizations, the greater biological effect per dose unit will be achieved [11, 13].

The ability to produce multiple ionizations within a short distance is the reason why IR can generate clustered damage on both DNA strands in close proximity. The unique ability of IR to produce DSBs is the major reason for its toxicity and ability to induce mutations and cancer.

The DNA damage clusters induced by IR can be divided into non-DSB-containing clusters, like base damage to both strands or one-strand break opposed by base damage, as well as DSB-containing clusters with a DSB in combination with oxidative base damage, AP sites, and SSBs [11, 12]. The complexity of the lesions increases as the linear energy transfer (LET) of IR increases. For low LET, 30-40% of the DNA damage consists of complex DSBs as opposed to 90% for high LET [14]. Accordingly, biological consequences such as mutagenesis, lethality and reduced repair of DSBs increase with increasing LET.

Figure 4. Different types of ionizing radiation-induced clustered DNA damage. B stands for base damage. Aida Muslimović, published in Current Topics in Ionizing radiation Research, 2012, p.4.

1.2.5 DNA-damaging drugs

While IR induces a broad spectrum of oxidative DNA damage in addition to SSBs and DSBs, chemotherapeutic drugs work through different mechanisms like alkylation, cross-linking, inhibition of the DNA synthesis, induction of SSBs and DSBs by free radicals and interaction with topoisomerases. Many chemotherapeutic drugs do not induce DSBs directly, but other lesions that can be transformed into DSBs once the cells try to go through DNA replication.

Alkylating drugs

Alkylating drugs are electrophilic compounds that react with nucleophilic centers in the DNA, mostly nitrogen-7 of the base rings and oxygen in the phosphodiester bonds. Alkylation also weakens the N-glykosidic bond which can lead to depurination/depyrimidination and the formation of AP sites.

Alkylating drugs can be mono- and bi-functional, meaning that they interact with one or two bases in the DNA, which can lead to intra-strand and inter-strand cross links. These types of DNA damage inhibit DNA replication and DNA transcription and are toxic if not repaired [2].

Cross-linking drugs

The cross-linking drug cisplatin can induce intra-strand adducts if they are positioned on the same strand, or inter-strand cross-links if they are positioned on two opposite strands. Inter-strand cross-links are particularly toxic, as they lead to complete blockage of both DNA replication and transcription. In addition, inter-strand cross-links involve both strands in the DNA, making repair of this type of damage complicated [2].

Antimetabolites

Antimetabolites are substances that resemble precursors to DNA or RNA. Treatment with antimetabolites can lead to incorporation of the wrong nucleotides or block the DNA synthesis. One example is the purine-analog tioguanine that becomes phosphorylated in the cell. During the S-phase the tri-phosphorylated form of the drug can become incorporated into DNA or inhibit DNA polymerase. Pyrimidine analogs like gemcitabine are cytidine analogs that inhibit the synthesis of deoxy-nucleotide triphosphates in addition to being incorporated in DNA resulting in chain-termination and mutations [11, 13].

Radiomimetic drugs

Free radical-based DNA-cleaving drugs, like bleomycin, neocarzinostatin and calicheamicin act through direct cleavage of DNA. Bleomycin becomes activated by chelation with iron and can then abstract hydrogen atoms from C4 in DNA resulting in formation of SSBs, DSBs and abasic sites. Calicheamicin γ-1 (CLM) is an enediyne antibiotic that contains a biradical center. CLM binds to the minor groove in the DNA and is thereby positioned close to the backbone. Reduction of the trisulfide in the molecule leads to cooperative activation of two radical centers in the molecule. The radicals then abstract hydrogen atoms from the sugar backbone, which results in cleavage of the DNA, preferentially at TCCT-AGGA sequences [2, 15]. Close to 30% of all CLM-induced DNA strand breaks are DSBs [16], as compared to 10% by bleomycin and 1-3% by IR, making CLM one of the most potent DSB-inducing drugs known.

Topoisomerase inhibitors

Topoisomerase inhibitor drugs like campthothecin and etoposide generate SSBs and DSBs by inhibition of Topoisomerase I or II, respectively [17].

Topoisomerase II (TopoII) normally makes transient protein-linked DSBs in order to resolve knots and tangles in the DNA ahead of replication forks, during separation of two sister chromatids and during meiosis. Topo II is a homodimer, each monomer of which makes staggered nicks in the DNA, by formation of a transient covalent bond between the formed 5' phosphate overhangs and the active site tyrosyls in the protein [18]. Normally, after passage of an undamaged DNA molecule through the break, Topo II religates the break and dissociates from the DNA [19]. However, in the presence of etoposide, this religation is inhibited and Topo II will remain linked to the breaks [20]. Topo II can be denatured after collision with RNA and DNA polymerases, which blocks religation [21, 22]. In order to detect and repair these denatured DSBs, Topo II must first be removed, which is probably done by proteasome degradation [23-25], endonucleolytic processing [26] and tyrosyl-DNA phosphodiesterase cleavage [27, 28]. After removal of topo II, DSBs are repaired by a process involving Ku and Ligase IV (ligIV).

1.3 DNA damage repair

Several defense mechanisms protect us from spontaneous DNA damage. For instance, the packaging of DNA into the cell nucleus, far away from oxygen-consuming mitochondria and peroxisomes reduces contact with oxygen. In addition, the compact package of DNA into chromatin protects DNA from contact with ROS. Iron storages like ferritin and transferrin reduce ROS production. Specialized enzymes like superoxide dismutase (SOD), peroxidases and peroxiredoxin proteins help to limit the DNA exposure to ROS. Cells also have multiple DNA damage repair mechanisms [2] that cope with DNA damage on daily basis.

Most DNA-damaging agents like ROS and alkylating drugs induce single-stranded DNA damage leaving the opposite strand intact. This type of damage is quickly repaired by template-directed DNA repair systems like base excision repair (BER) and nucleotide excision repair (NER). In BER, the damaged base is initially excised after which the damaged DNA backbone is removed and replaced by newly synthesized DNA. Bulkier DNA lesions like pyrimidine dimers and alkyl groups that distort the structure of the DNA helix are preferentially repaired by NER. The process starts by excision of a short region of DNA that contains the lesion, thereafter the

remaining complementary strand is used as a template to synthesize the removed strand [2].

1.4 DSB repair

In mammalian cells, DSBs are repaired by two main pathways: homologous recombination (HR) and non-homologous end joining (NHEJ) [29].

1.4.1 Homologous recombination

HR is most prominent during mitosis, S and G2 phases when an identical sister chromatid is available as a template for the recombination process [30]. HR is therefore considered to be the error-free repair pathway.

Homologous recombination is initiated by MRN complex binding to DNA ends. Mre11 can based on the type of the lesion form two different complexes, a synaptic or a branched complex [31]. The synaptic complex is formed between Mre11 and double-stranded DNA with short 3´ overhangs resembling the DSB. The branched complex is formed between Mre11 and both double-stranded and single-stranded DNA resembling a stalled replication fork. The endonuclease activity of Mre11 allows opening of the DNA double helix, while the MRN 5´-3´ exonuclease activity initiates the DSB resection. DSB resection also requires C-terminal binding protein interacting protein (CtIP) in the S and G2 phases of the cell cycle and CtIP has been shown to interact with Mre11[32]. Other nucleases like ExoI and Dna2 also seem to be involved in DSB resection and Blooms syndrome helicase (BLM) seems to interact with replication protein A (RPA) [33, 34]. The resulting 3´-ssDNA overhangs are coated by the ssDNA-binding protein (RPA), which is subsequently replaced by Rad51. After homology searching, the Rad51 nucleoprotein filament mediates strand invasion of the homologous sister chromatid, resulting in formation of a Holliday junction [35]. DNA synthesis is then performed by DNA polymerases δ and η followed by ligation by DNA Ligase I and resolution of the Holliday junctions by BLM [36, 37].

1.4.2 Non-homologous end joining

NHEJ is the main pathway for DSB repair in mammalian cells, as most of our cells are in the G1 and G0 phases where HR is suppressed [30]. Most of the DSBs contain abnormal nucleotides at the ends and are not directly ligatable. Therefore, the DNA ends must be processed prior to ligation, which may result in loss of nucleotides and deletion mutations. NHEJ is therefore considered to be an error-prone repair pathway. In NHEJ DNA-ends are first detected and processed to remove damaged nucleotides followed by DNA synthesis and ligation. The proteins known to participate in NHEJ are DNA-dependent protein kinase (DNA-PK), Artemis, polynucleotide kinase (PNK), Aprataxin and PNK-like factor (APLF), X-ray cross-complementing 4 (XRCC4), XRCC4-like factor (XLF)/(Cernunnos), and DNA Ligase IV (LigIV).

DNA-PK consists of the DNA-binding subunit Ku70/80 heterodimer (Ku), and the catalytic subunit DNA-PKcs. Ku is recruited to DSBs seconds after DSB induction and binds specifically to the DNA ends through a preformed channel [38-40]. Once bound to DNA ends, Ku translocates inwards from the DNA ends, allowing one DNA-PKcs molecule to bind to each DNA end [41, 42] and to form a synaptic complex that brings the two DNA ends into close proximity of each other [42], resulting in activation [43-45] and autophosphorylation [46] of the DNA-PK holoenzyme. DNA-PKcs autophosphorylation is thought to be required for the conformational change between opened and closed holoenzyme conformations, which causes release of the DNA ends and is required for the further recruitment of NHEJ proteins for end processing by polynucleotide kinase (PNK), polymerization by the DNA polymerases μ or γ and, finally, ligation by the LigIV/XRCC4 complex and XLF/Cernunnos [47-50]. DNA-PKcs also binds to and activates the nuclease Artemis, which is believed to be involved in the end processing of more complex DSBs [6, 51-53]. Cells treated with inhibitors of DNA-PK kinase activity are more radiosensitive compared to cells lacking DNA-PKcs expression and also have slower HR. Cells expressing mutant forms of DNA-PKcs, where serine residues in the ABCDE phosphorylation cluster that are targets of DNA-PK autophosporylation have been mutated to alanine, are more radiosensitive than cells not expressing DNA-PKcs [54]. These findings indicate that DNA-PK kinase activity is required for dissociation of DNA-PKcs that otherwise blocks further processing and ligation of the DNA ends [55].

Deletion or inhibition of the core components of NHEJ Ku, DNA-PKcs, XRCC4, LigIV, Artemis and XLF/Cernunnos leads to sensitivity to IR and other DSB-inducing agents as well as defective V(D)J recombination and DSB repair.

There is an alternative NHEJ (B-NHEJ) pathway that becomes activated when the classical NHEJ (D-NHEJ) pathway is defective [29]. Cells defective in DNA-PKcs, Ku and LigIV repair all IR-induced DSBs, albeit with slower kinetics [56-58]. Moreover, cells defective in HR components like Rad51B, Rad52 and Rad54 display repair kinetics similar to the wild type, indicating that HR is not responsible for the slower repair mechanism observed in NHEJ-deficient cells [57]. In alternative NHEJ, Poly [ADP-ribose] polymerase 1 (PARP1) binds to DNA ends instead of Ku [59] and the DNA-ligases I and III (LigI and LigIII) [60] and X-ray repair cross-complementing 1 (XRCC1) LigIII/XRRC1 complex ligates the breaks [61]. The Mre11-Rad50-Nbs1/Nibrin complex (MRN) may also be involved as a substitute for Artemis [62-65]. The alternative NHEJ is believed to be error-prone, as it can require microhomology for the end joining, which can result in chromosomal translocations and rearrangements [66].

1.4.3 DSB repair in the context of heterochromatin

DSBs are repaired by two distinct kinetics. Approximately 85% of IR-induced DSBs are repaired rapidly within 10-30 minutes while 15% of the DSBs are repaired in a slower manner and can take up to 24h [67, 68]. For long, the complexity of the DSBs has been thought to be the main reason for this dual kinetic profile. However, recent studies suggest that chromatin compaction and the presence of heterochromatin might be the major factor influencing the repair rate [69], and that DSBs with different chemical complexities of the DNA ends induced by the free radical-inducing drug neocarzinostatin and an oxidative damaging agent, tert-butyl hydroperoxide (TBH), are repaired with similar kinetics as IR-induced DSBs [69, 70]. Also, the slowly repaired DSBs induced by IR, neocarzinostatin and TBH accumulate at heterochromatic regions. The general consensus is therefore that DSBs are repaired slowly in HC and rapidly in EC. The slow component of DSB repair is defective in cells lacking Ataxia-telangiectasia-mutated (ATM) or the nuclease Artemis. In the G1/G0 phases of the cell cycle, both ATM and Artemis are therefore required for the slow component of DSB repair in

addition to other DSB-involved proteins like LigIV, DNA-PKcs and histone H2AX (H2AX), MRN, mediator of DNA damage checkpoint protein 1 (MDC1), Ring finger protein 8 (RNF8), Ring finger protein 168 (RNF168) and p53-binding protein 1 (53BP1) required for signaling [71, 72]. Furthermore, (Krüppel-associated box)-zinc finger protein-associated protein 1 (KAP1), an HC-building factor, was found to be involved in HC-DSB repair. Cells with a single mutation in the phosphorylation site Ser824 of KAP1 are sensitive to the radiomimetic drug neocarzinostatin [73]. ATM phosphorylates KAP1 on Ser824 [69, 73], which leads to the formation of pan-nuclear P-KAP1 and P-KAP1-foci. Pan-nuclear P-KAP1 formation does not involve 53BP1 in contrast to P-KAP1 foci formation, indicating that P-KAP1 foci are required for the repair of HC-DSBs [72]. KAP1 is initially phosphorylated minutes after DSB induction and then spreads throughout the chromatin [73]. Also, ATM-dependent Kap1 phosphorylation has been linked to chromatin relaxation [69, 73] after DSB induction, indicating that phosphorylation of KAP1 may facilitate the accessibility of DSB in HC. In addition, KAP1 phosphorylation seems to disturb interactions between chromodomain-helicase-DNA-binding protein 3 (CHD3) and small ubiquitin-related modifier 1 **(**SUMO1) resulting in spreading of CHD3 from HC followed by chromatin relaxation and DSB repair [74]. None of the abovementioned factors are required for the repair of EC-DSBs that are rapidly rejoined in G1 and G2 by NHEJ. With all this in mind, the prevailing theory is that the slowly repaired DSBs are localized to HC and signaled in an ATM-dependent manner and repaired by NHEJ including Artemis in G1 and by HR in G2, while the rapidly repaired DSBs are localized to euchromatin and repaired by NHEJ.

1.5 DSB response and H2AX phosphorylation

1.5.1 H2AX phosphorylation

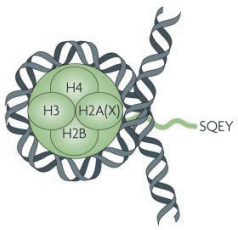

One of the first cellular responses to DSBs is phosphorylation of histone H2AX [75], which is one of the most evolutionary conserved H2A variants that constitutes 2-25% of all nucleosomes [76]. The highly conserved SQEY motif positioned in the carboxy terminal of H2AX contains serine 139 that becomes phosphorylated upon DSB induction[75, 77].

Figure 5. Nucleosome with H2AX and SQEY-tail. Adapted with permission from Nature reviews cancer; "γ-H2AX and cancer", Bonner, W.M. et al, p.960.

Thousands of H2AX molecules become phosphorylated over a 2Mbp region flanking the DSB within minutes of DSB induction, resulting in the formation of gamma-H2AX foci, P-H2AX foci [77] that most likely represent single DSBs [78, 79]. The SQEY phosphorylation motif in H2AX is the common recognition site for Ataxia-telangiectasia-mutated (ATM), DNA-dependent protein kinase (DNA-PK) and ATM, and ataxia telangiectasia and Rad-3-related (ATR) kinases belonging to the phosphatidylinositol-OH-kinase-like family of protein kinases (PIKKs), which can all phosphorylate H2AX [80]. ATM and DNA-PK can both phosphorylate H2AX redundantly upon induction of DSBs in G1 and G2 [81, 82].

ATR, on the other hand, phosphorylates H2AX upon replication stress and UV damage during the S phase [83-85]. ATR is activated by ssDNA regions via a process that requires ATR-interacting protein (ATRIP) and RPA binding to the ssDNA regions [86].

1.5.2 DSB recognition and signaling

DSBs are initially recognized by the Mre11-Rad50-Nbs1/Nibrin complex (MRN). The Rad50/Mre11 binds to DNA ends via its central globular domain and binds DNA ends with the flexible arms of multiple Rad50/Mre11 complexes [87]. NBS1 binds ATM leading to ATM activation [88, 89]. ATM activation is believed to occur in two steps, where MRN-dependent DNA binding first increases the local concentration of DNA ends and induces ATM monomerization, followed by ATM activation and autophosphorylation[90]. ATM is rapidly autphosphorylated on serine 1981 after irradiation of cells [91]. The requirement of autophosphorylation for ATM activation and monomerization is, however, unclear, as ATM mutated in serine 1981 to alanine is capable of phosphorylating p53 and checkpoint kinase 2 (Chk2) in its dimeric form [89]. On the other hand, it was shown that ATM autophosphorylation on Ser1981 leads to dimer dissociation and monomerization of ATM [91]. Nevertheless, activation of ATM leads to phosphorylation of downstream targets that initiate cell cycle arrest, DNA repair or cell death like by (Chk2), (p53) and H2AX.

Initial ATM/MRN dependent H2AX phosphorylation serves as a marker for the mediator of DNA damage checkpoint protein 1 (MDC1) that, in its phosphorylated form, binds to the phospho-group of H2AX [92]. MDC1 also binds to NBS1/Nibrin [93] of the MRN complex, leading to additional

recruitment of ATM to the DSB site and resulting in extension of the H2AX phosphorylation signal to more distal chromatin regions flanking the DSB. Extension of the H2AX phosphorylation signal also occurs after replication stress where MDC1 recruits topoisomerase II β-binding protein (TopBP1) [94] that binds and activates ATR, which then continues to phosphorylate H2AX.

MDC1 binding to P-H2AX can apparently also be affected by other H2AX phosphorylations, like Tyr 142, that is constitutively phosphorylated by the Williams-Beuren syndrome transcription factor (WSTF) [95]. Tyr 142 phosphorylation results in binding of the proapoptotic kinase JNK1 or mitogen-activated kinase 8 (MAPK8) instead of MDC1. A protein tyrosine phosphatase, (EYA) has been shown to dephosphorylate Tyr 142, at least in embryonic kidney cells, leading to recruitment of MDC1 [96]. This could reflect a mechanistic link to the observation that DNA damage signaling can contribute to both survival and apoptosis in response to DNA damage.

1.5.3 DNA damage checkpoints

DNA damage induces cell cycle checkpoints at the G1/S and G2/M transitions and in the S phase. The cell cycle checkpoints prevent the cells from performing DNA replication and cell division in the presence of DNA damage, as that would pass on the DNA damage to daughter cells resulting in mutations and chromosomal rearrangement. Depending on the extent of the DNA damage, the cells either repair the damage and proceed through the cell cycle, permanently arrest the cell cycle (senescent cells) or die by induction of apoptosis.

Depending on the cell cycle phase, different pathways will preferentially be activated. The G1/S checkpoint is regulated by CyclinD/Cdk4 (cyclin-dependent kinase 4) and CyclinE/Cdk2 (cyclin-dependent kinase 2) and prevents cells from entering into the S phase and initiating DNA replication. G1 cells exposed to DSBs can inactivate CyclinE/Cdk2 in two ways [97, 98]. One mechanism involves ATM, which activates Chk2 by phosphorylation at Thr-68. This leads to degradation of Cdc25A (cell division cycle 25) and persistent inhibitory phosphorylation of Cdk2 causing checkpoint arrest. The second mechanism involves phosphorylation of p53 and its negative regulator Mdm2 by ATM and Chk2, resulting in p53 activation and stabilization. This leads to p53 transcriptional activation of p21 (cyclin-

dependent kinase inhibitor 1), which binds to and inhibits the cyclinE/Cdk2 complex causing checkpoint arrest.

The G2/M checkpoint is regulated by the CyclinB1/Cdk1 (cyclin-dependent kinase 1) complex and prevents cells from entering mitosis and dividing. DSBs in G2 activate ATM that phosphorylates Chk2. Chk2 phosphorylates Cdc25A, leading to cytoplasmatic translocation of Cdc25A and inhibition of CyclinB1/Cdk1 and finally G2 arrest [98].

Upon DNA damage in the S phase, ATM or ATR are activated depending on the type of DNA damage (DSBs or replication fork stalling) and, in turn, activate Chk1 and Chk2. Similar to the G1/S checkpoint, ATM blocks DNA replication origin firing via Chk2 activation that phosphorylates Cdc25A, leading to its degradation and subsequent accumulation of inhibitory phosphorylation on Cdk2. ATR-dependent Chk1 activation leads to inhibition of Cdc25A, first by Cdc25A phosphorylation and subsequent degradation, but also through Cdc25A C terminal phosphorylation that inhibits CdC25A to dephosphorylate Cdk2 [99].

1.5.4 Chromatin modifications associated with the DSB response

DNA damage signaling and repair processes must have access to DNA in order to repair the damage. Since DNA is tightly packed around the nucleosomes in the chromatin, several chromatin modifications like acetylation, ubiquitylation and SUMOylation take place in order to make the DNA more accessible to DNA repair proteins.

Histone acetylation has been implicated in the DNA damage response to DSBs. Histone acetylations are regulated by histone acetyl transferases (HATs) and histone deacetylases (HDACs) that add and remove acetyl groups from lysine residues. Histone acetyl transferase tat-interactive protein 60 (Tip60) has been shown to acetylate H2AX, leading to H2AX ubiquitylation by ubiquitin-conjugating enzyme 13 (Ubc13) after IR [100]. Tip60 interacts with H2AX immediately after IR and interacts with ubiquitin-conjugating enzyme 13 (Ubc13). The Tip60-Ubc13 complex then induces acetylation of H2AX on lysine 5 (K5), followed by ubiquitylation of H2AX. This H2AX ubiquitylation causes release of H2AX from the chromatin into the un-irradiated area. It is therefore believed that as H2AX phosphorylation

marks the DSB site for the recruitment of ATM/MRN and MDC1, the H2AX acetylation followed by ubiquitylation marks the H2AX release from the DSB site to allow access of the repair proteins to the DSB.

Ubiquitylation is a process that involves E1, E2 and E3 protein ligases that ubiquitylate other proteins by covalent attachment of a 76 amino acid-long polypeptide, either in monomeric or polymeric form. As ATM/MRN initiates the first wave of protein accumulation at the DSB site, the second wave of proteins starts by binding of RING finger-containing nuclear factor 8 (RNF8) to phosphorylated MDC1 [101]. RNF8 then interacts with the E3 ubiquitin ligase HERC2, which facilitates interaction with E2 ubiquitin-conjugating enzyme (Ubc13). This assembly of proteins leads to recruitment of an additional ubiquitin ligase RNF168 that has been found mutated in patients with RIDDLE syndrome, resulting in radiosensitivity, immunodeficiency and dysmorphic features. RNF168 interacts with Ubc13, leading to lysine 63-linked polyubiquitylation of histones H2A and H2AX[102]. This polyubiquitylation serves as a recruitment platform for p53-binding protein 1 (53BP1) and breast cancer type 1 susceptibility protein (BRCA1) [103, 104]. BRCA1 forms a complex with receptor-associated protein 80 (Rap80) [105] and Abraxas [106] and localizes to DSBs via ubiquitin-interacting motif (UIM) in Rap80 and lysine 63-linked ubiquitin chains [107]. Recruitment of BRCA 1 and 53BP1 also requires SUMO E3 ligases PIAS1 and PIAS4, and both SUMO1 and SUMO2/3 accumulate around the DSB site [108, 109]. PIAS4-mediated SUMOylation also seems to be important for RNF168 accumulation at the DSB sites [108].

1.6 P-H2AX foci formation and elimination

Initially, P-H2AX foci are formed as small, distinct foci at the DSB, with half-maximum numbers reached 1-3 minutes after irradiation. After the initial H2AX phosphorylation and MDC1-mediated positive feedback loop that loads additional ATM and MRN to the DSB site, the P-H2AX foci grow in size and H2AX phosphorylation spreads along the chromatin upstream from the two DNA ends. The maximum amount of P-H2AX in the cell is reached after 30-60 minutes[75, 77, 78]. Depending on the celline, 0.03-0.06% of H2AX molecules per DSB become phosphorylated and spread over 2 Mbp regions of chromatin-containing ~2000 P-H2AX molecules[75]. However, phosphorylated P-H2AX regions can reach up to 30Mbp from the DSB [77, 79], resulting in amplification of the DSB signal to large chromatin regions.

Several reports have described large persistent P-H2AX foci that are present for several hours [110-112] up to days after irradiation[113].

P-H2AX could be eliminated by direct histone dephosphorylation or dephosphorylation after histone exchange with unphosphorylated H2AX. The histone exchange rate is slow, but correlates with the rejoining rate of slowly repaired DSBs (half-time 3-4h) and may be possible for P-H2AX removal [114]. For instance, PPC2 has been co-purified with H2A-H2B histone dimer and may be involved in the dephosphorylation of dissociated H2A-H2B and the incorporation of the unphosphorylated H2A-H2B into the nucleosome [115]. However, the current model dictates that P-H2AX is removed via a direct dephosphorylation mechanism. Four serine/threonine phosphatases have been reported to dephosphorylate H2AX in human cells: PP2A, PP4, PP6 and PP2C. PP2A dephosphorylates H2AX at the site of the DSB and siRNA knockdown of the catalytic subunit of PP2A leads to persistence of foci and inefficient DSB repair [116]. PP4 associates with chromatin and dephosphorylates chromatin-bound H2AX molecules phosphorylated by ATR during replication [117-119]. PP6 also dephosphorylates H2AX [119] and knockdown of its catalytic subunit results in persistent gamma-H2AX and 53BP1 foci. PP2A and PP6 seem to be involved in the recovery from the G2/M checkpoint. Recently, (wild-type-53-induced phosphatase) WIP1 has been reported to dephosphorylate H2AX, resulting in suppression of the DSB repair and termination of the cell cycle checkpoints [120, 121].

1.7 Defects in DSB signaling and repair pathways

Inborn errors in DNA damage signaling or repair lead disorders with instable chromosomes, cancer and in many cases neurological defects. For instance, individuals with Ataxia telangiectasia (A-T) disorder born with mutations in the ATM gene, are predisposed to lymphoma and leukemia and display neurodegeneration and immunodeficiency [122, 123]. A-T cells are hypersensitive to IR and have defective cell cycle checkpoints as well as spontaneous chromosome rearrangements. Ataxia telangiectasia-like disorder (ATLD) connected with hypersensitivity to IR and genomic instability is another disease where the mutated gene is Mre11, a component of the MRN complex that, together with ATM, sense DSBs [123]. Another MRN complex component, NBS1, is mutated in Nijmegen breakage syndrome that is associated with

genomic instability, IR sensitivity, immunodeficiency, predisposition to lymphoma and neurodegeneration [123].

Severe combined immunodeficiency (SCID) is a disorder resulting from defects in components of V(D)J recombination and NHEJ. There are two groups of SCID patients, those who have a signaling defect (T-B+SCID) and those with a defect in V(D)J recombination (T-B-SCID). In T-B-SCID, most mutations are found in Rag1 and Rag2 genes [124]; however, mutations in Artemis [125-128], LigIV [129, 130] and XLF/Cernunnos [47, 131] genes have been found in radiosensitive SCID patients. The latter defect also leads to growth retardation and microcephaly and T and B cell lymphocytopenia. DNA-PKcs mutations leading to SCID have been known for long in mice, dogs, horses and human cellines [132-135]. However, mutations in human patients have until recently been unknown. A DNA-PKcs mutation has recently been found in a radiosensitive T-B-SCID human patient [136]. The mutation did not interfere with DNA-PKcs activity or autophosphorylation; however, it resulted in inefficient Artemis activation and consequently disturbed the coding joint formation and reduced the number of B and T cells. Ku70, Ku86 and XRCC4 mutations have not been found in humans either. However, Ku70 and Ku86 knockout mice are viable, but have growth retardation, premature senescence and RS-SCID [137-139]. Human cellines with null mutations in Ku70 and Ku86 [140] are not viable. Homozygous deletion of the XRCC4 gene in mice leads to embryonic lethality, owing to apoptosis of post-mitotic neurons.

Recently, ubiquitin ligase RNF168, required for the recruitment of 53BP1 to DSB sites has been found mutated in patients with RIDDLE syndrome, much similar to A-T disorder. RIDDLE patients are characterized by radiosensitivity, and immunological and neurological defects [103, 141, 142].

1.8 P-H2AX detection

Immunofluorescence microscopy

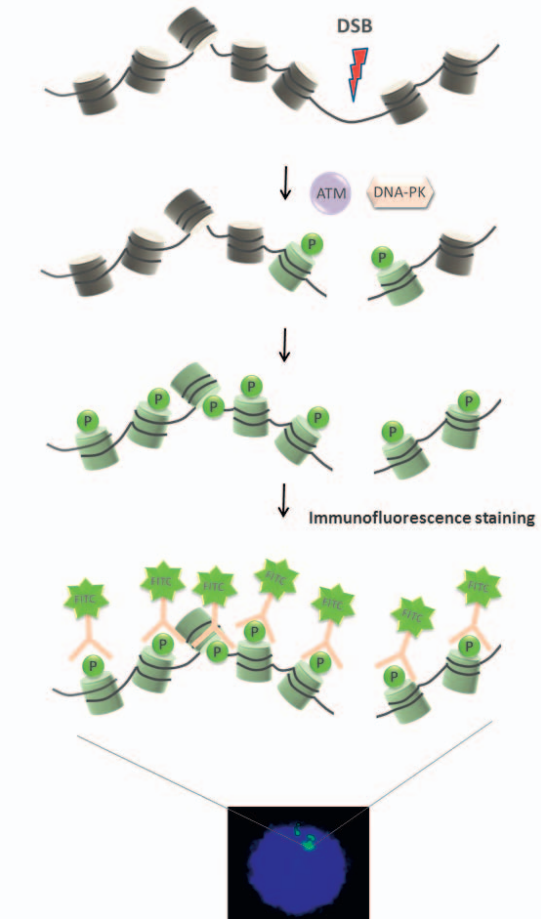

Using phosphospecific antibodies it is possible to measure H2AX phosphorylation by Western blot, flow cytometry and immunofluorescence. However, the most sensitive method for P-H2AX detection is currently immunofluorescence microscopy, as it enables quantification of single P-H2AX foci in individual cells reflecting the numbers of actual DSBs. The level of P-H2AX induced by drugs and irradiation is closely correlated to the level of cell death induced by IR and other DSB-inducing agents [143, 144]. It is therefore possible that measurement of P-H2AX could be used as a measure of the toxic effects of DSB-inducing agents in cancer patients. In immunofluorescence, fixed cells or tissue are attached to glass slides and incubated with P-H2AX antibodies. After staining procedures with secondary antibodies and DNA dyes, the slides are dried and mounted with cover glasses before analysis by fluorescence microscopy (Fig 6). The whole procedure is labour-intensive and often takes a day or more to finalize.

Figure 6. P-H2AX foci formation and detection. Aida Muslimović, published in Current Topics in Ionizing radiation Research, 2012, p.9.

P-H2AX foci can be quantified either by manual counting in a fluorescence microscope or by foci counting software from digital images. Either way has its advantages and difficulties. Manual foci counting is probably the most accurate way to quantify the number of foci in a cell. This method is,

however, time-consuming, as hundreds of cells must be counted for statistical reliability. Foci-quantifying software, on the other hand, is challenged by the heterogeneous nature of P-H2AX foci, which may vary both in size and brightness. Therefore, multiple foci located in close proximity of each other can be mistaken for single foci by the foci-counting software. This is particularly common after high radiation doses when over 20-40 foci are formed in each cell nucleus and after high LET radiation that generates multiple DSBs in a dense area. Other difficulties can arise by focusing problems due to digital photos being taken in single plane, which can affect the size and brightness of the foci. Using automated scanning microscopes in addition to foci-quantifying software could be a possible clinical approach for foci quantification during therapy.

Flow cytometry

Flow cytometry has also been used to measure the P-H2AX signal. However, the possibility of detecting single P-H2AX foci and DSBs is lost with flow cytometry. Instead, the P-H2AX phosphorylation signal from the whole cell in a large population is measured. The flow cytometry method is faster and less labour-intensive but also less sensitive, compared with detection of P-H2AX foci by immunofluorescence microscopy. Briefly, in the flow cytometry method, cells are stained and permeabilized in a staining buffer containing fluorescently labelled P-H2AX antibodies and DNA dyes. The samples can be analysed immediately after staining, and the data delivered in the same day. Due to its simplicity, this method can be implemented in its current form in clinical laboratories where flow cytometers are often available.

An important shortcoming of the flow cytometry method is its low analytical sensitivity compared with counting of separate P-H2AX foci. A contributing factor to the low sensitivity is that undamaged cells have a diffuse background signal from the P-H2AX antibodies. The nature of this background is unclear but results in a requirement of at least 2-5 P-H2AX foci per cell to separate the signal from undamaged cells. At low IR doses (<0.1Gy), most cells contain 0-1 foci per nucleus. The sensitivity of the foci method relies on its ability to score cells with one focus among cells without foci. Radiation doses generating an increase from one focus in every 20 cells (0.05 foci/cell) to one focus in every 10 cells (0.1 foci/cell) yield a significant increase that can be scored with the foci method. In contrast, this increase remains below the detection limit in the flow cytometer, as the P-H2AX signal from cells with 1-2 foci is not separated from undamaged cells. For that reason, flow cytometry analysis can only measure the P-H2AX signal at

IR doses over 0.1-0.3 Gy (unpublished data), whereas the foci method can measure in the mGy range [145].

On the other hand, most radiotherapy regimens include fractionated doses of 1.5-5 Gy. For the subset of mononuclear cells residing in the irradiated area, this dose is well within the measurable range for flow cytometry analysis. In addition, flow cytometry allows analysis of small subsets of P-H2AX-positive cells, as up to 100 000 cells are analysed in each sample. This is particularly helpful when mononuclear cells are analysed from patients following local irradiation, where blood cells from the irradiated area are mixed with unirradiated cells.

1.8.1 Clinical applications of P-H2AX detection

Immunofluorescence microscopy and P-H2AX foci counting have been used both *in vitro* and in patients to measure DNA damage following radiotherapy and chemotherapy. Initial studies using low doses of irradiation of human fibroblast cultures showed that there was a correlation between the IR dose, the numbers of P-H2AX foci, and the number of DSBs. This study also established that increased levels of P-H2AX foci are detectable at doses as low as 1mGy [145]. The ability to detect very low levels of radiation has inspired the use of P-H2AX foci in mononuclear cells from patients exposed to X-rays in computerized tomography (CT) [146] and other X-ray examinations. P-H2AX foci analysis was used as a biomarker for individual radiation damage in pediatric patients undergoing cardiac catheterization, showing that previous estimates according to the linear-no-threshold hypothesis have underestimated the radiation damage. Therefore, P-H2AX foci analysis could be used as a tool for estimations of DNA damage effects after cardiac catheterization [147]. Another study showed that the number of P-H2AX foci in lymphocytes after coronary CT angiography is correlates to the dose-length product (DLP), which is a physical parameter used to calculate the delivered dose after CT. Therefore, P-H2AX foci analysis could be used to measure individual dose-related effects of X-rays [148]. P-H2AX foci analysis has also been used for estimations of individual radiation doses by comparisons of lymphocytes exposed *in vivo* and *in vitro* to fractionated irradiation or angiography, indicating that P-H2AX foci analysis could be used for dose estimations [149]. In addition, several reports now show that P-H2AX foci analysis can be used to measure DNA damage induced by local

radiotherapy. Analysis of P-H2AX foci in prostate cancer biopsies after *in vivo* radiation showed reproducible quantifications of foci numbers in prostate specimens in the dose region 0-1Gy [150]. P-H2AX foci has also been be used to follow induction of DNA damage in lymphocytes of cancer patients with different cancer types who were exposed to local radiotherapy treatments in different sites of the body. There was a correlation between the mean number of P-H2AX foci per lymphocyte and the integrated total body radiation dose, indicating that measurements of P-H2AX foci in lymphocytes can be used for *in vivo* dosimetry [151]. Immunofluorescence microscopy has also been successful in the detection of the DSB response after treatment with cancer drugs, like the Topoisomerase-I inhibitor camptothecin [152], in human biopsies [150], circulating tumor cells [153], lymphocytes and plucked hair bulbs [154]. A fully automated high-throughput system, the RABIT (Rapid Automated Biodosimetry Tool), has been developed for P-H2AX analysis of human lymphocytes and can process several thousands of blood samples per day, which might be useful in larger nuclear accidents[155]. Finally, it was reported that radio-immuno conjugates with a peptide that allows cellular uptake of labelled the P-H2AX antibody could be used to measure P-H2AX foci in living cells and in whole mice. The method was less sensitive than conventional P-H2AX foci staining in fixed and permeabilized cells, but this technique opens up the interesting possibility of monitoring DSB induction in patient tumors by imaging techniques, such as gamma camera or even magnetic resonance tomography (MRT), in the future [156].

Flow cytometry measurements of P-H2AX have been used to diagnose Ataxia telangiectasia, a disease where patients are radiosensitive and show a delayed clearance of P-H2AX foci after *in vitro* irradiation of lymphocytes [157]. Similar methods have been used to find patients with severe normal tissue toxicity following radiotherapy [158], and to study the P-H2AX response in several subsets of nucleated blood cells [159]. However, so far, apart from the pilot study of rectal cancer patients receiving pelvic irradiation [160], no clinical study has used flow cytometry to measure P-H2AX levels in patient samples after radiotherapy.

P-H2AX analysis has also been used in genotoxicity measurements with ELISA-based assays [161] and high content screening assays [162].

1.9 Cancer and treatment

Second only to surgery, the most common cancer treatment is DNA damage therapy, used in over 50% of all cancer cases at some point. Radiotherapy and several chemotherapeutic drugs kill cancer cells by cutting cellular DNA right off, producing DNA double-strand breaks (DSBs), the most toxic DNA damage type.

Only 1-10 DSBs are enough to induce permanent cell cycle arrest and clonogenic cell death in human cells [5]. However, the clinical effects of radiation and chemotherapy are highly variable among patients. Today, radiation and chemotherapy doses are derived empirically from population averages in sensitivity, so that some patients will be extremely sensitive and experience severe side effects while others will receive suboptimal doses and low tumor effect. Radiation and chemotherapy are usually planned during 1-3 weeks and delivered over a period of weeks to months. DNA damage testing of the patients could be performed as a part of the therapy planning. The level of DNA damage could be measured after the first dose of chemotherapy or radiation, to allow personalized dosing during the following weeks of treatment.

Induction of a DSB is followed by rapid P-H2AX phosphorylation that can be measured by flow cytometry and immunofluorescence microscopy. P-H2AX phosphorylation levels have been shown to correlate well with the level of cell death induced by radiation or chemotherapy [143, 144]. Measurements of P-H2AX response could therefore be a possible approach to monitor DSBs in cancer patients during treatment with radiotherapy or chemotherapy as a way to personalize the dosing.

Peripheral blood mononuclear cells are well suited for this purpose for several reasons. Blood collection is not as invasive as biopsies and poses little risk to patients. Mononuclear cells can be prepared within 30 minutes and over a million cells can be obtained from each millilitre of blood. In addition, the flow cytometry P-H2AX assay is able to measure the P-H2AX signal at IR doses of over 0.1-0.3 Gy and the P-H2AX foci method is able to measure in the mGy range [145]. As most radiotherapy regimens include fractionated doses of 1.5-5 Gy, both flow cytometry and immunofluorescence microscopy are within the measurable range. In addition, flow cytometry allows analysis of small subsets of P-H2AX-positive cells, as hundreds of thousands of cells can be analysed in each sample. This is particularly helpful

when mononuclear cells are analysed from patients following local irradiation, where blood cells from the irradiated area are mixed with un-irradiated cells.

Conventional radiotherapy and chemotherapy could probably be further optimized if dosing was based on individual sensitivity to DNA damage. P-H2AX analysis opens, for the first time, the possibility to measure DNA damage during cancer treatment.

2 AIM

The overall aim of my research has been to develop and validate methods to measure P-H2AX in mononuclear cells from cancer patients undergoing radiotherapy.

2.1 Specific Aims

1. To characterize DNA damage induced by the chemotherapeutic drug etoposide and test its ability to induce P-H2AX response using a flow cytometry-based P-H2AX assay.

2. To optimize the flow cytometry assay for measurements of P-H2AX response in mononuclear cells from cancer patients undergoing radiation therapy.

3. To develop calibrators for the flow cytometry analysis of P-H2AX in order to implement the method in the clinic.

4. To optimize the immunofluorescence p-H2AX method foci counting methods for the clinical setting.

3 METHODS

3.1 Cell maintenance and culture

All cell cultures were kept in a 5% CO_2 incubator at 37ºC. Cells were trypsinized in PBS containing 0.25% trypsin and 0.5mM EDTA and always transferred to new bottles upon reaching confluence. Cells were grown in an appropriate medium recommended by the Coriell Institute for Medical Research and American type culture collection (ATCC).

3.2 Colony-forming survival assay *Paper I*

Clonogenic survival after treatment with cytostatics CLM and etoposide was determined by colony-forming survival assay. Cells were treated with CLM or etoposide for 40 minutes before washing and trypsinization. Cells were serially diluted and plated at different densities and grown for two weeks in normal growth medium to allow the colonies to expand. Cells were then fixed in methanol and stained with Giemsa before colony counting by eye. Smaller colonies were examined in a microscope. A colony was defined as a coherent assembly of more than 50 cells.

3.3 Patients and collection of samples *Paper II, III, IV*

Blood samples were collected in EDTA tubes from three rectal cancer patients before and 1 h after radiation. The patients were treated in a linear accelerator with 6 and 15 MV photons. The blood samples were kept on ice after collection during all storage and handling steps. One portion of the blood samples was irradiated *in vitro* with a dose range used for the *in vivo* treatments. *In vitro* radiation of blood was carried out with an RT-100 Superficial Therapy X-ray (Philips, the Netherlands) with 100 kVp, 8 mA and 1.7 mm aluminum filter, as previously described. The dose rate was 1.46 Gy/min and the focus-to-target distance was 30 cm. Mononuclear cells were prepared by the lymphoprep procedure (Axis-Shield) immediately after blood collection of the *in vivo* samples, while *in vitro*-irradiated samples were incubated for 30 min at 37°C to induce H2AX phosphorylation prior to the preparation of mononuclear cells. The patients gave their written informed consent, and the procedure was approved by the regional ethics committee in Gothenburg, Sweden.

3.4 Detection of DNA strand breaks
Paper I

3.4.1 Neutral and alkaline constant field gel electrophoresis (CFGE)

DSBs were measured by neutral constant field gel electrophoresis (neutral CFGE). After drug exposure, the cells were kept on ice until scraping, and all solutions added to the cells were ice-cold. Cells were treated with CLM and etoposide for 40 min at 37°C. The cells were harvested and suspended in PBS and mixed with an equal volume of melted agarose and transferred to a plug mold to solidify on ice for at least 10 minutes. The gel plugs were then lysed in a proteinase-K and SDS-containing buffer. The plugs were then equilibrated for 1.5h to remove SDS and proteinase K, molded into an agarose gel and subjected to constant field gel electrophoresis for 17h. The gels were stained with ethidium bromide and analyzed using a fluorescence scanner. The relative amount of cellular DNA migrating into the gel, fraction of activity released, FAR, was quantified using Image Quant 5.2. Briefly, the background-subtracted signal in a rectangle covering the gel plug and the DNA that migrated into the gel was considered as the "total DNA signal." The background-subtracted signal from a smaller rectangle drawn 1 mm below the gel plug covering the DNA that entered the gel was considered as the "fraction of activity released." FAR was calculated using the following equation: FAR = activity released/total DNA signal.

3.4.2 Alkaline constant field gel electrophoresis (CFGE)

TSBs (DSBs + SSBs) were measured by alkaline CFGE method, as described above for neutral CFGE with modifications after the deproteinization procedure. Plugs were equilibrated for an additional 1.5h in alkaline buffer in order to unwind both DNA strands and reveal TSBs. The plugs were then molded into a 0.7% agarose gel mixed in water the day before and equilibrated in alkaline buffer (0.03 M NaOH, 2 mM EDTA, 0.5 M NaCl) overnight at 4°C. The assembled alkaline gel was run at 4°C for 17 h at 0.6 V/cm in alkaline buffer (0.03M NaOH, 2mM EDTA (pH 12.5)) directly. The

relative amounts of DSBs and SSBs were calculated by comparing extrapolations from the linear part of the etoposide and CLM FAR plot with IR, as the number of DSBs and TSBs is known for 1Gy of IR. The FAR value from the neutral CFGE and alkaline CFGE was used to find a drug concentration that produced a FAR value corresponding to 1 Gy. SSBs were calculated with the formula: SSB=TSB-DSB.

3.5 Detection of P-H2AX response

3.5.1 Flow cytometry *Paper I, II, III*

The total H2AX phosphorylation signal in a cell population was analysed by flow cytometry. Cell or bead suspensions were added to a detergent-containing buffer with a FITC-conjugated mouse monoclonal P-H2AX antibody and stained in the dark for 3h at 4°C in Papers I and II and for 1h on a rock at 4°C in Paper III. Cell cycle distribution was monitored by addition of a DNA stain (Vybrant dye cycle violet stain. In Paper I we analysed the distribution of the P-H2AX signal during the cell cycle and sorted out cells in the G1, S and G2 phases, based on the DNA content, and analysed for DNA strand breaks. The P-H2AX analysis in Paper I was done by FACSAria. Later analyses of control cells and beads were performed on a C6-Accuri flow cytometer. The fluorescence intensity was plotted in histograms and the mean fluorescence intensity was calculated using the Weasel version 2.3 software or CFlow Plus Analysis software.

3.5.2 Immunofluorescence microscopy *Paper IV*

P-H2AX foci analysis was performed by immunofluorescence microscopy in Paper IV. Unless otherwise indicated, all steps were carried out on ice or at 4°C. Mononuclear cells ($50\text{-}100\times10^3$) were fixed in paraformaldehyde (PFA), permeabilized and stained in solution with the primary P-H2AX antibody by gentle inversion of the tubes for 1h at 4°C. The cells were then washed and stained in solution with the secondary antibody by gentle inversion of the tubes for 30 min at 4 °C. After centrifugation and removal of the supernatant,

the cells were suspended in a spotting buffer based on water, BSA and Triton X-100, in order to avoid formation of salt crystals during the drying step. Five µl of the cell suspension was spotted onto a microscope slide and allowed to air-dry for 30 min, creating a cell 'spot'. The dried slides were fixed in acetone-methanol and air-dried briefly. The nuclei were then stained with Hoechst 33342 by incubation of slides with Hoechst dye for 3 min, washed twice with dH2O, dried briefly, and mounted with a cover glass using fluorescence mounting medium (Dako). However, the Hoechst dye can be added to the secondary antibody solution, eliminating this step. P-H2AX foci were counted manually from 50 or 100 cells from digital images taken with a wide-field fluorescence microscope (100×objective) and processed with ImageJ software (free software provided by the National Institutes of Health).

4 RESULTS AND DISCUSSION

4.1 Paper I

Etoposide is a cancer drug that induces strand breaks in cellular DNA by inhibiting topoisomerase II (TopoII) religation of cleaved DNA [163]. Although DNA cleavage by Topo II always produces Topo II-linked DNA double-strand breaks (DSBs), the action of etoposide also results in single-strand DNA breaks (SSB), since religation of the two strands are independently inhibited by etoposide. Previous studies indicate that Topo II-linked DSBs must be denatured by colliding RNA or DNA polymerases, followed by removal of the denatured Topo II to allow for detection of the DSBs. These studies therefore suggest that detection of etoposide-induced DNA strand breaks require elaborate processing to allow for the detection and possible repair of the Topo II-linked DNA breaks.

Initially, we wanted to characterize DNA damage induced by etoposide and test its ability to induce a P-H2AX response using a flow cytometry-based P-H2AX assay.

To examine this in cells we have measured the relative amount of SSBs and DSBs in cells treated with etoposide. We found that only 3 % of the DNA strand breaks induced by etoposide were DSBs. We also measured the relative survival following treatment with etoposide and CLM, a drug that introduce naked radical-induced DSBs. In the same cell population we measured DSBs, SSBs and H2AX phosphorylation, a DSB-specific DNA damage signal. We found that etoposide-induced DSBs were more than ten times less toxic than CLM-induced DSBs. This difference was explained by a tenfold difference in H2AX phosphorylation at a given DSB level. We found that most, possibly over 90 %, of the DSBs produced by etoposide failed to activate any DSB response. It is therefore likely that most etoposide-induced DSBs are held in Topo II-linked complexes that fail to be recognized by ATM, DNA-PK and other DNA damage recognition systems. Likely, these DSBs are religated by topoisomerase II itself and are therefore not relying on the cellular DSB repair systems, like non-homologous end joining. The remaining 10 % of etoposide-induced DSBs are converted to naked DSBs, probably by RNA/DNA polymerases and proteasomes and can possibly induce other DNA damage recognition systems.

We also wanted to examine if etoposide-induced DNA strand breaks and H2AX phosphorylation are more prominent in the S phase of the cell cycle, as topoisomerases are active in the S phase where they help to relieve torsional stress ahead of the replication forks. CLM, on the other hand, cleaves DNA by a radical-mediated process, and is not expected to induce DSBs in a cell cycle–dependent manner. We therefore sorted cells treated with etoposide or CLM in the G1, S, and G2 phases using FACS according to the DNA content, and measured the level of DSBs by neutral CFGE and H2AX phosphorylation. We found similar levels of DSB and H2AX phosphorylation throughout the cell cycle for both etoposide and CLM. Therefore, it is unlikely that different toxicities of etoposide and CLM depend on the cell cycle distribution.

Previous reports have indicated that etoposide-induced DSBs must be denatured by RNA or DNA polymerases and that Topo II moiety must be removed in order to induce H2AX phosphorylation [23-25], which could result in delayed H2AX phosphorylation as opposed to CLM that generates protein-free DSBs. We therefore measured H2AX phosphorylation and DSBs by neutral CFGE at different time points and found that the DSB level reached a maximum after 20 min and H2AX phosphorylation after 40 min in CLM-treated cells. However, in etoposide-treated cells, the maximum DSB level was reached after 40 min, but H2AX phosphorylation reached its maximum after 160 min, reflecting the extended time required for processing of Topo II-linked DNA ends.

In conclusion, these data indicate that etoposide mostly induces Topo II-linked SSBs that contribute little, if anything, to the toxicity. Of the few DSBs that are produced, less than 10 % result in a DSB response via H2AX phosphorylation and consequently toxicity. Therefore, measurement of the P-H2AX response might be a good measure of etoposide induced toxicity.

4.2 Paper II

Histone H2AX is rapidly phosphorylated in response to DSBs [77]. DSB induction and repair could therefore be observed via H2AX phosphorylation. We wanted to optimize the flow cytometry assay for measurements of P-H2AX response in mononuclear cells from cancer patients undergoing radiation therapy.

In this assay, the cells are stained and permeabilized in a staining buffer containing fluorescently labelled gamma-H2AX antibodies and DNA dyes. After staining for 15 minutes up to a few hours, the samples can be analysed directly by flow cytometry without further processing. In flow cytometry, up to 100 000 cells can be analysed in each sample within minutes, allowing detection of even small subsets of gamma-H2AX-positive cells.

To verify that the assay can be used to monitor the DSB response in patient mononuclear cells, blood samples were collected before and after 5Gy pelvic irradiation. We also irradiated patient blood *in vitro* with the same dose and used this as an internal control. Mononuclear cells were prepared and labeled with a phospho-specific antibody against P-H2AX and analyzed by flow cytometry. We found that approximately 5 % of the mononuclear cells retrieved one hour after the pelvic irradiation had the same P-H2AX signal as cells irradiated with 5 Gy *in vitro*. These cells were probably trapped in the microcirculation in the irradiated area and therefore received the full 5Gy dose. This pilot study indicated that flow cytometry may be well suited for the measurement of P-H2AX induction in mononuclear blood cells following local radiotherapy.

4.3 Paper III

To be able to implement measurements of the P-H2AX-response in clinical practice and to relate the extent of P-H2AX to the clinical outcome and side effects we have also characterized calibrators for the flow cytometry analysis based on phosphopeptide-coated beads and fixed cells. Calibrators are necessary for inter-lab comparisons and to monitor day-to-day assay variations.

Control beads were generated by mixing streptavidin-coated magnetic beads with a biotinylated phosphopeptide derived from H2AX, followed by drying and storage at room temperature. Control cells were generated from primary human fibroblasts treated with the DSB-inducing drug CLM for 30 minutes, followed by fixation and storage in 90% EtOH at -70°C. Both controls were stable over 40 days and were equally capable of correcting the P-H2AX signal from two different antibody batches.

In order to test whether control cells and beads could be used for corrections of day-to-day variations, we irradiated mononuclear cells from three healthy individuals and analyzed the P-H2AX signal on different days together with control beads and cells. Using correction factors generated from control cells close to the P-H2AX signal in each sample, it was possible to correct for day-to-day variations.

Both the control beads and cells performed equally well with respect to correcting for assay variations. The control beads might be more suitable for clinical use, as they are easy to manufacture in large quantities and can be shipped at ambient temperature, thereby facilitating inter-laboratory comparisons. However, a potential problem with the beads is that they do not present the antigen in a way that resembles the cellular structure in fixed cells. For this reason, we also established conditions that allowed fixed cells to serve as controls. Control cells, on the other hand, are difficult to produce in large numbers and must be shipped on dry ice that could make inter-laboratory calibrations impractical. In conclusion, we believe that control beads and cells can be used as internal controls for the flow cytometry P-H2AX assay.

4.4 Paper IV

The most sensitive method for measurements of the P-H2AX response is immunofluorescence microscopy-based foci detection, which enables quantification of single P-H2AX foci in individual cells. The method is labor-intensive and time-consuming, mainly due to the inconvenience of staining cells on microscope slides and manual counting of hundreds of cells. In order to adapt the immunofluorescence method to clinical settings in addition to automatic microscopic systems, we have developed a modification of the P-H2AX immunofluorescence method.

Instead of conventional staining of the cells on glass slides, we stained fixed mononuclear cells with fluorescent P-H2AX antibodies in solution before attaching them to microscope slides by drying a droplet of the cell sample in a salt-free protein solution.

We tested the in-solution staining on two cancer patient samples 1h after a 2Gy irradiation and used *in vitro*-irradiated patient blood as a control.

Mononuclear cells were prepared and stained with the in-solution procedure and 200 cells were counted manually. As expected, we were able to detect a subset of mononuclear cells with P-H2AX foci in the blood sample drawn 1h after irradiation, reflecting the circulating fraction of the cells in the irradiated volume at the time of irradiation. The P-H2AX foci numbers obtained from in-solution staining correlated well with the conventional staining on slides. In addition, we have established control cells adapted for the in-solution staining immunofluorescence microscopy. These control cells preserved their P-H2AX morphology and brightness after the fixing and freezing procedure.

We have set up an in-solution staining procedure that allows arraying of up to 16 patient samples per slide ready for foci counting in two hours. Together with automatic microscopic foci counting systems that are available [146], this new staining method holds great promise for the future implementation of the P-H2AX foci analysis in clinical routine practice.

5 FUTURE DIRECTIONS

Conventional radiotherapy and chemotherapy might be further optimized if dosing was based on the level of DNA damage and individual sensitivity to DNA damage. As we have observed in our previous studies [160, 164], P-H2AX analysis of patient blood during radiotherapy by flow cytometry and immunofluorescence microscopy could be used as a way to measure the extent of DSBs induced by the therapy. In radiotherapy, a predetermined radiation dose is delivered to a defined volume of the body, including the target tumor, during 5-10 minutes. Blood cells passing through the irradiated volume are exposed to variable doses and intermixed in the circulation with non-irradiated cells. Therefore, it is not clear if the foci counting or flow cytometry method could detect those P-H2AX-positive cells.

In a preliminary study, we have compared the P-H2AX foci counting and flow cytometry measurements of P-H2AX in an *in vitro*-generated mixture of irradiated and non-irradiated blood cells and blood cells recovered from cancer patients receiving a defined radiation dose. We found that foci counting was ten times more sensitive than flow cytometry and was able to detect an increase in P-H2AX foci over non-irradiated cells at a dose of 0.01 Gy. However, we found that the flow cytometry method was close to ten times more sensitive at detecting cells with increased P-H2AX levels when irradiated cells were mixed with non-irradiated cells to mimic the situation in patients. We also found that over 1000 cells must be analyzed to detect cells with elevated P-H2AX foci levels from irradiated patients, which is difficult to do by manual foci counting. Therefore, P-H2AX foci counting method can only be implemented in the clinic in a setting with automatic foci counting capabilities. Using the flow cytometry method we were able to detect elevated levels of P-H2AX in 8 of 11 cancer patients receiving ionizing radiation treatment. The 3 negative patients had received low radiation doses delivered in multiple small fractions. This preliminary study indicated that the inter-sample variation in signal intensity was the major reason for the flow cytometry methods inability to detect elevated P-H2AX signal in patients.

Thus, we need to further minimize the inter-sample variation in the flow cytometry method. One possible approach could be to use stained un-irradiated mononuclear cells as controls together with patient mononuclear cells in the same tube. The unirradiated cells could be specifically stained with a fluorescent red dye before mixing with the irradiated cells from the

same patient. If the red fluorescence does not interfere with the green fluorescence from the p-H2AX antibody, this could be used to separate, or gate, unirradiated control cells from irradiated cells by the flow cytometer software. In that way the control cells and the patient cells after irradiation would be contained in the same tube, possibly limiting the problem with inter-sample variation. In the following step, a series of mononuclear cells irradiated *in vitro* with different doses be analyzed together with red-stained un-irradiated cells to find the lowest dose that gives a detectable P-H2AX signal. Finally, the stained control cells could be tested in a larger patient group receiving varying radiation doses to different body volumes.

6 POPULÄRVETENSKAPLIG SAMMANFATTNING

Strålbehandling och cellgifter som används i över 50 % av alla cancerfall dödar cancerceller genom att skada deras DNA. Tyvärr skadas också normala cellers DNA vilket leder till svåra biverkningar. Man måste därför dosera precis rätt för att få effekt på tumören utan att orsaka för svåra skador. Denna finstämda dosering misslyckas ofta eftersom olika människor är olika känsliga för strålning och cellgifter och rensar ut cellgifter ur kroppen olika effektivt. Idag har man därför justerat doserna så att många sannolikt får för låga doser och otillräcklig effekt på tumören för att inte allvarligt skada de mest känsliga patienterna.

Målet med vår forskning har varit att utveckla metoder för att mäta hur väl patienten har svarat på stråL- eller cellgiftsbehandlingen för att kunna individanpassa doseringen under pågående behandling.

Fosforylerat H2AX (P-H2AX) är ett protein som markerar att DNA:t har blivit skadat genom dubbelsträngsbrott (DSB). Genom att mäta P-H2AX i blodprov från patienter som precis har fått sin behandling, kan man få en uppfattning om hur mycket behandlingen har skadat cancercellerna och justera doserna så att varje patient får behandling som är anpassat till just hennes/hans tumörrespons. På detta sätt blir patientens vita blodceller reporterceller för hur mycket DNA-skada som har bildats i det bestrålade området.

Vi har optimerat en flödescytometribaserad metod för att mäta fosforylerat H2AX i vita blodceller från cancerpatienter under pågående strålbehandling. P-H2AX signalen mätt med denna metod korrelerade väl med toxiska effekter av etoposid som är en av de mest använda cellgifterna i cancerbehandlingen. Med denna metod kunde vi mäta celler innehållande P-H2AX i 3 rektalcancerpatienter. För att metoden ska kunna användas kliniskt på ett pålitligt sätt så har vi även utvecklat kontrollceller och plastkulor som kan användas för att justera dag-till-dag variation i metoden. Vi har också optimerat en mikroskopibaserad metod för mätning av enskilda P-H2AX i patienternas prover som kan användas i de patientfall där flödescytometrimetoden inte är tillräckligt känslig. Denna metod är uppbyggd så att multipla patientprover ska kunna analyseras samtidigt i ett automatiskt immuno-fluorescens-mikroskop samt med en foci-räknande mjukvara.

Under behandlingen, som ofta pågår flera veckor, kan cancerläkaren ta nya blodprov och löpande mäta hur mycket DNA-skador som bildats i patientens blodceller. Läkaren kan då under behandlingen justera doserna upp eller ner så att precis rätt mängd skadat DNA bildas under behandlingen. Vi tror att denna möjlighet kommer att öka möjligheten att bota utan att skada vid cancerbehandling.

7 ACKNOWLEDGEMENTS

I would like to thank everybody that have been involved and followed me on this incredible journey!

First of all, my supervisor Ola Hammarsten, I could write many pages full with thanks for everything that you have taught me during all these years, but there is simply not enough space. First of all, thank you for giving me the opportunity for a fantastic PhD-period in your research group! Thank you for your endless support and encouragement and for believing in me, even when I did not believe in myself. Thank you for always being understanding even throughout the tough times. I will forever be impressed by your great knowledge and research strategies and by your way of managing work and family.

My cosupervisor Ragnar Hultborn, thank you for your invaluable help with our patient studies and for the fun meetings and discussions.

Erik Fernström, thank you for all your help with collection of the patient samples and for always being willing to help.

To all my friends and colleagues at the Clinical Chemistry department, many thanks for all the nice lunches and coffee breaks. Special thanks to Ruth Wickelgren and Ulla Strandberg for all the administrative help. Katarina Junevik, many thanks for your help with the FACSAria.

My room-mates, Alexandra Abramsson, Annica Sjölander, Cecilia Boreström Sherin Matthews, Susanne Nyström and Åsa Nilsson, thank you for all your advices and cheers!

Pegah Johansson, thank you for the time we have worked together. We have achieved a lot during our late hours.

Sherin Matthews and Karin Starnberg, thank you for this fun time and all your help. Good luck to you with your PhD:s.

Kristina Eriksson and Merita Idriz, thank you for making the time in the lab so much fun!

Ismail Hassan Ismail, thank you for helping me set up my very first experiments in the lab and for always being willing to discuss with me,

whatever the issue. Thank you for always being so helpful and kind and for guiding me in the right direction. The lab was simply not the same when you left. Finally, thank you for being a friend.

Susanne Nyström, thank you for introducing me into the lab, teaching me new techniques and for your invaluable help with experiments. Thank you for being a friend, always caring and ready to listen and share everyday life happenings and our childrens adventures. Finally, thank you for all the encouraging words and messages when I was about to give up.

Malin, Sara and Petra, without you guys, this would not have been as fun as it was. Malin von Otter and Sara Landgren, thank you for our small getaways and presents that always made my day. Petra Bergström, thank you for your friendship and constructive critics on almost anything. Thank you for making an effort in understanding my background and following me to my home country.

To all my dearest friends and family outside the lab, thank you for cheering me on and for asking if I have gotten any results yet.

To my parents in law and brother in law, Mirjana, Emir and Zlatan, thank you for being interested in my studies and for all you help and support.

My dearest brother and Miki thank you for all your help and for taking Emina on fun adventures during this period. Dado, thank you for always believing in me, looking up to me and for taking my mind of work by taking me to Paris! You are the best brother in the whole world!

My dearest parents, I cannot explain how grateful I am for you and how much I love and respect you! I am so blessed to have you as my parents! Thank you for your endless love, your self-less giving, your never-ending support and understanding. Thank you for always thinking of me and Dado first and for giving us everything that you possibly can. Thank you for always guarding us and for giving us an innocent and pleasant childhood despite everything. You are truly the best parents in the world and I love you so much!

My dearest husband, Darmin, you always know how to cheer me up make me smile. Thank you for your patience and love. My dearest Emina, you are the brightest star in my universe and my greatest wish coming true! Thank God I have you! You are perfect and I love you so much.

REFERENCES

1. Mathews C.K., H.K.E., Ahern K. G. Biochemistry (Robin Heyden, Addison Wesley Longman Inc. Benjamin/Cummings, San Francisco, CA, 2000).
2. Friedberg E. C., W.G.C., Siede W., Wood R. D., Schultz R. A., Ellenberger T. DNA Repair and Mutagenesis (ASM Press, Washington DC, USA, 2006).
3. Geoffrey M. Cooper, R.E.H. The Cell: A Molecular Approach (ASM Press, Sinnauer Associates, 2007).
4. Van Der Schans, G.P. Gamma-ray induced double-strand breaks in DNA resulting from randomly-inflicted single-strand breaks: temporal local denaturation, a new radiation phenomenon? *Int J Radiat Biol Relat Stud Phys Chem Med* **33**, 105-20 (1978).
5. Huang, L.C., Clarkin, K.C. & Wahl, G.M. Sensitivity and selectivity of the DNA damage sensor responsible for activating p53-dependent G1 arrest. *Proc Natl Acad Sci U S A* **93**, 4827-32 (1996).
6. Ma, Y., Pannicke, U., Schwarz, K. & Lieber, M.R. Hairpin opening and overhang processing by an Artemis/DNA-dependent protein kinase complex in nonhomologous end joining and V(D)J recombination. *Cell* **108**, 781-94 (2002).
7. Gellert, M. V(D)J recombination: RAG proteins, repair factors, and regulation. *Annu Rev Biochem* **71**, 101-32 (2002).
8. Soulas-Sprauel, P. et al. V(D)J and immunoglobulin class switch recombinations: a paradigm to study the regulation of DNA end-joining. *Oncogene* **26**, 7780-91 (2007).
9. Keeney, S. & Neale, M.J. Initiation of meiotic recombination by formation of DNA double-strand breaks: mechanism and regulation. *Biochem Soc Trans* **34**, 523-5 (2006).
10. Neale, M.J. & Keeney, S. Clarifying the mechanics of DNA strand exchange in meiotic recombination. *Nature* **442**, 153-8 (2006).
11. J., H.E. Radiobiology for the Radiologist (Lippincott Williams & Wilkins, Philadelphia, PA, 2000).
12. Magnander, K. & Elmroth, K. Biological consequences of formation and repair of complex DNA damage. *Cancer Lett* (2012).
13. Onkologi. Onkologi (Liber AB, Stockholm, 2008).
14. Nikjoo, H., O'Neill, P., Terrissol, M. & Goodhead, D.T. Quantitative modelling of DNA damage using Monte Carlo track structure method. *Radiat Environ Biophys* **38**, 31-8 (1999).
15. Zein, N., Poncin, M., Nilakantan, R. & Ellestad, G.A. Calicheamicin gamma 1I and DNA: molecular recognition process responsible for site-specificity. *Science* **244**, 697-9 (1989).

16. Elmroth, K., Nygren, J., Martensson, S., Ismail, I.H. & Hammarsten, O. Cleavage of cellular DNA by calicheamicin gamma1. *DNA Repair (Amst)* **2**, 363-74 (2003).
17. Burden, D.A. & Osheroff, N. Mechanism of action of eukaryotic topoisomerase II and drugs targeted to the enzyme. *Biochim Biophys Acta* **1400**, 139-54 (1998).
18. Liu, L.F., Rowe, T.C., Yang, L., Tewey, K.M. & Chen, G.L. Cleavage of DNA by mammalian DNA topoisomerase II. *J Biol Chem* **258**, 15365-70 (1983).
19. Berger, J.M., Gamblin, S.J., Harrison, S.C. & Wang, J.C. Structure and mechanism of DNA topoisomerase II. *Nature* **379**, 225-32 (1996).
20. Osheroff, N. Effect of antineoplastic agents on the DNA cleavage/religation reaction of eukaryotic topoisomerase II: inhibition of DNA religation by etoposide. *Biochemistry* **28**, 6157-60 (1989).
21. D'Arpa, P., Beardmore, C. & Liu, L.F. Involvement of nucleic acid synthesis in cell killing mechanisms of topoisomerase poisons. *Cancer Res* **50**, 6919-24 (1990).
22. Bodley, A.L., Huang, H.C., Yu, C. & Liu, L.F. Integration of simian virus 40 into cellular DNA occurs at or near topoisomerase II cleavage hot spots induced by VM-26 (teniposide). *Mol Cell Biol* **13**, 6190-200 (1993).
23. Desai, S.D., Li, T.K., Rodriguez-Bauman, A., Rubin, E.H. & Liu, L.F. Ubiquitin/26S proteasome-mediated degradation of topoisomerase I as a resistance mechanism to camptothecin in tumor cells. *Cancer Res* **61**, 5926-32 (2001).
24. Mao, Y., Desai, S.D., Ting, C.Y., Hwang, J. & Liu, L.F. 26 S proteasome-mediated degradation of topoisomerase II cleavable complexes. *J Biol Chem* **276**, 40652-8 (2001).
25. Zhang, A. et al. A protease pathway for the repair of topoisomerase II-DNA covalent complexes. *J Biol Chem* **281**, 35997-6003 (2006).
26. Neale, M.J., Pan, J. & Keeney, S. Endonucleolytic processing of covalent protein-linked DNA double-strand breaks. *Nature* **436**, 1053-7 (2005).
27. Nitiss, K.C., Malik, M., He, X., White, S.W. & Nitiss, J.L. Tyrosyl-DNA phosphodiesterase (Tdp1) participates in the repair of Top2-mediated DNA damage. *Proc Natl Acad Sci U S A* **103**, 8953-8 (2006).
28. Pouliot, J.J., Yao, K.C., Robertson, C.A. & Nash, H.A. Yeast gene for a Tyr-DNA phosphodiesterase that repairs topoisomerase I complexes. *Science* **286**, 552-5 (1999).
29. Mladenov, E. & Iliakis, G. Induction and repair of DNA double strand breaks: the increasing spectrum of non-homologous end joining pathways. *Mutat Res* **711**, 61-72.

30. Rothkamm, K., Kruger, I., Thompson, L.H. & Lobrich, M. Pathways of DNA double-strand break repair during the mammalian cell cycle. *Mol Cell Biol* **23**, 5706-15 (2003).
31. Rupnik, A., Lowndes, N.F. & Grenon, M. MRN and the race to the break. *Chromosoma* **119**, 115-35 (2010).
32. Sartori, A.A. et al. Human CtIP promotes DNA end resection. *Nature* **450**, 509-14 (2007).
33. Mimitou, E.P. & Symington, L.S. Nucleases and helicases take center stage in homologous recombination. *Trends Biochem Sci* **34**, 264-72 (2009).
34. Brosh, R.M., Jr. et al. Replication protein A physically interacts with the Bloom's syndrome protein and stimulates its helicase activity. *J Biol Chem* **275**, 23500-8 (2000).
35. San Filippo, J., Sung, P. & Klein, H. Mechanism of eukaryotic homologous recombination. *Annu Rev Biochem* **77**, 229-57 (2008).
36. Chu, W.K. & Hickson, I.D. RecQ helicases: multifunctional genome caretakers. *Nat Rev Cancer* **9**, 644-54 (2009).
37. Mohaghegh, P., Karow, J.K., Brosh, R.M., Jr., Bohr, V.A. & Hickson, I.D. The Bloom's and Werner's syndrome proteins are DNA structure-specific helicases. *Nucleic Acids Res* **29**, 2843-9 (2001).
38. Mimori, T. & Hardin, J.A. Mechanism of interaction between Ku protein and DNA. *J Biol Chem* **261**, 10375-9 (1986).
39. de Vries, E., van Driel, W., Bergsma, W.G., Arnberg, A.C. & van der Vliet, P.C. HeLa nuclear protein recognizing DNA termini and translocating on DNA forming a regular DNA-multimeric protein complex. *J Mol Biol* **208**, 65-78 (1989).
40. Walker, J.R., Corpina, R.A. & Goldberg, J. Structure of the Ku heterodimer bound to DNA and its implications for double-strand break repair. *Nature* **412**, 607-14 (2001).
41. Hammarsten, O., DeFazio, L.G. & Chu, G. Activation of DNA-dependent protein kinase by single-stranded DNA ends. *J Biol Chem* **275**, 1541-50 (2000).
42. DeFazio, L.G., Stansel, R.M., Griffith, J.D. & Chu, G. Synapsis of DNA ends by DNA-dependent protein kinase. *EMBO J* **21**, 3192-200 (2002).
43. Meek, K. New targets to translate DNA-PK signals. *Cell Cycle* **8**, 3809 (2009).
44. Meek, K., Gupta, S., Ramsden, D.A. & Lees-Miller, S.P. The DNA-dependent protein kinase: the director at the end. *Immunol Rev* **200**, 132-41 (2004).
45. Gottlieb, T.M. & Jackson, S.P. The DNA-dependent protein kinase: requirement for DNA ends and association with Ku antigen. *Cell* **72**, 131-42 (1993).

46. Mahaney, B.L., Meek, K. & Lees-Miller, S.P. Repair of ionizing radiation-induced DNA double-strand breaks by non-homologous end-joining. *Biochem J* **417**, 639-50 (2009).
47. Ahnesorg, P., Smith, P. & Jackson, S.P. XLF interacts with the XRCC4-DNA ligase IV complex to promote DNA nonhomologous end-joining. *Cell* **124**, 301-13 (2006).
48. Li, Z. et al. The XRCC4 gene encodes a novel protein involved in DNA double-strand break repair and V(D)J recombination. *Cell* **83**, 1079-89 (1995).
49. Critchlow, S.E., Bowater, R.P. & Jackson, S.P. Mammalian DNA double-strand break repair protein XRCC4 interacts with DNA ligase IV. *Curr Biol* **7**, 588-98 (1997).
50. Grawunder, U. et al. Activity of DNA ligase IV stimulated by complex formation with XRCC4 protein in mammalian cells. *Nature* **388**, 492-5 (1997).
51. Drouet, J. et al. Interplay between Ku, Artemis, and the DNA-dependent protein kinase catalytic subunit at DNA ends. *J Biol Chem* **281**, 27784-93 (2006).
52. Goodarzi, A.A. et al. DNA-PK autophosphorylation facilitates Artemis endonuclease activity. *EMBO J* **25**, 3880-9 (2006).
53. Wang, J. et al. Artemis deficiency confers a DNA double-strand break repair defect and Artemis phosphorylation status is altered by DNA damage and cell cycle progression. *DNA Repair (Amst)* **4**, 556-70 (2005).
54. Ding, Q. et al. Autophosphorylation of the catalytic subunit of the DNA-dependent protein kinase is required for efficient end processing during DNA double-strand break repair. *Mol Cell Biol* **23**, 5836-48 (2003).
55. Allen, C., Halbrook, J. & Nickoloff, J.A. Interactive competition between homologous recombination and non-homologous end joining. *Mol Cancer Res* **1**, 913-20 (2003).
56. Nevaldine, B., Longo, J.A. & Hahn, P.J. The scid defect results in much slower repair of DNA double-strand breaks but not high levels of residual breaks. *Radiat Res* **147**, 535-40 (1997).
57. Wang, H. et al. Efficient rejoining of radiation-induced DNA double-strand breaks in vertebrate cells deficient in genes of the RAD52 epistasis group. *Oncogene* **20**, 2212-24 (2001).
58. Wang, H. et al. Genetic evidence for the involvement of DNA ligase IV in the DNA-PK-dependent pathway of non-homologous end joining in mammalian cells. *Nucleic Acids Res* **29**, 1653-60 (2001).
59. Wang, M. et al. PARP-1 and Ku compete for repair of DNA double strand breaks by distinct NHEJ pathways. *Nucleic Acids Res* **34**, 6170-82 (2006).

60. Liang, L. et al. Human DNA ligases I and III, but not ligase IV, are required for microhomology-mediated end joining of DNA double-strand breaks. *Nucleic Acids Res* **36**, 3297-310 (2008).
61. Audebert, M., Salles, B. & Calsou, P. Involvement of poly(ADP-ribose) polymerase-1 and XRCC1/DNA ligase III in an alternative route for DNA double-strand breaks rejoining. *J Biol Chem* **279**, 55117-26 (2004).
62. Rahal, E.A. et al. ATM regulates Mre11-dependent DNA end-degradation and microhomology-mediated end joining. *Cell Cycle* **9**, 2866-77 (2010).
63. Xie, A., Kwok, A. & Scully, R. Role of mammalian Mre11 in classical and alternative nonhomologous end joining. *Nat Struct Mol Biol* **16**, 814-8 (2009).
64. Rass, E. et al. Role of Mre11 in chromosomal nonhomologous end joining in mammalian cells. *Nat Struct Mol Biol* **16**, 819-24 (2009).
65. Deriano, L., Stracker, T.H., Baker, A., Petrini, J.H. & Roth, D.B. Roles for NBS1 in alternative nonhomologous end-joining of V(D)J recombination intermediates. *Mol Cell* **34**, 13-25 (2009).
66. McVey, M. & Lee, S.E. MMEJ repair of double-strand breaks (director's cut): deleted sequences and alternative endings. *Trends Genet* **24**, 529-38 (2008).
67. Lobrich, M., Rydberg, B. & Cooper, P.K. Repair of x-ray-induced DNA double-strand breaks in specific Not I restriction fragments in human fibroblasts: joining of correct and incorrect ends. *Proc Natl Acad Sci U S A* **92**, 12050-4 (1995).
68. Metzger, L. & Iliakis, G. Kinetics of DNA double-strand break repair throughout the cell cycle as assayed by pulsed field gel electrophoresis in CHO cells. *Int J Radiat Biol* **59**, 1325-39 (1991).
69. Goodarzi, A.A. et al. ATM signaling facilitates repair of DNA double-strand breaks associated with heterochromatin. *Mol Cell* **31**, 167-77 (2008).
70. Woodbine, L., Brunton, H., Goodarzi, A.A., Shibata, A. & Jeggo, P.A. Endogenously induced DNA double strand breaks arise in heterochromatic DNA regions and require ataxia telangiectasia mutated and Artemis for their repair. *Nucleic Acids Res* **39**, 6986-97 (2011).
71. Riballo, E. et al. A pathway of double-strand break rejoining dependent upon ATM, Artemis, and proteins locating to gamma-H2AX foci. *Mol Cell* **16**, 715-24 (2004).
72. Noon, A.T. et al. 53BP1-dependent robust localized KAP-1 phosphorylation is essential for heterochromatic DNA double-strand break repair. *Nat Cell Biol* **12**, 177-84 (2010).
73. Ziv, Y. et al. Chromatin relaxation in response to DNA double-strand breaks is modulated by a novel ATM- and KAP-1 dependent pathway. *Nat Cell Biol* **8**, 870-6 (2006).

74. Goodarzi, A.A., Kurka, T. & Jeggo, P.A. KAP-1 phosphorylation regulates CHD3 nucleosome remodeling during the DNA double-strand break response. *Nat Struct Mol Biol* **18**, 831-9 (2011).
75. Rogakou, E.P., Pilch, D.R., Orr, A.H., Ivanova, V.S. & Bonner, W.M. DNA double-stranded breaks induce histone H2AX phosphorylation on serine 139. *J Biol Chem* **273**, 5858-68 (1998).
76. Kinner, A., Wu, W., Staudt, C. & Iliakis, G. Gamma-H2AX in recognition and signaling of DNA double-strand breaks in the context of chromatin. *Nucleic Acids Res* **36**, 5678-94 (2008).
77. Rogakou, E.P., Boon, C., Redon, C. & Bonner, W.M. Megabase chromatin domains involved in DNA double-strand breaks in vivo. *J Cell Biol* **146**, 905-16 (1999).
78. Sedelnikova, O.A., Rogakou, E.P., Panyutin, I.G. & Bonner, W.M. Quantitative detection of (125)IdU-induced DNA double-strand breaks with gamma-H2AX antibody. *Radiat Res* **158**, 486-92 (2002).
79. Pilch, D.R. et al. Characteristics of gamma-H2AX foci at DNA double-strand breaks sites. *Biochem Cell Biol* **81**, 123-9 (2003).
80. Wang, H., Wang, M., Bocker, W. & Iliakis, G. Complex H2AX phosphorylation patterns by multiple kinases including ATM and DNA-PK in human cells exposed to ionizing radiation and treated with kinase inhibitors. *J Cell Physiol* **202**, 492-502 (2005).
81. Stiff, T. et al. ATM and DNA-PK function redundantly to phosphorylate H2AX after exposure to ionizing radiation. *Cancer Res* **64**, 2390-6 (2004).
82. Burma, S., Chen, B.P., Murphy, M., Kurimasa, A. & Chen, D.J. ATM Phosphorylates Histone H2AX in Response to DNA Double-strand Breaks*. *J Biol Chem* **276**, 42462-7 (2002).
83. Ward, I.M. & Chen, J. Histone H2AX is phosphorylated in an ATR-dependent manner in response to replicational stress. *J Biol Chem* **276**, 47759-62 (2001).
84. Ward, I.M., Minn, K. & Chen, J. UV-induced ataxia-telangiectasia-mutated and Rad3-related (ATR) activation requires replication stress. *J Biol Chem* **279**, 9677-80 (2004).
85. Furuta, T. et al. Phosphorylation of histone H2AX and activation of Mre11, Rad50, and Nbs1 in response to replication-dependent DNA double-strand breaks induced by mammalian DNA topoisomerase I cleavage complexes. *J Biol Chem* **278**, 20303-12 (2003).
86. Zou, L. & Elledge, S.J. Sensing DNA damage through ATRIP recognition of RPA-ssDNA complexes. *Science* **300**, 1542-8 (2003).
87. de Jager, M. et al. Human Rad50/Mre11 is a flexible complex that can tether DNA ends. *Mol Cell* **8**, 1129-35 (2001).
88. You, Z., Chahwan, C., Bailis, J., Hunter, T. & Russell, P. ATM activation and its recruitment to damaged DNA require binding to the C terminus of Nbs1. *Mol Cell Biol* **25**, 5363-79 (2005).

89. Lee, J.H. & Paull, T.T. ATM activation by DNA double-strand breaks through the Mre11-Rad50-Nbs1 complex. *Science* **308**, 551-4 (2005).
90. Dupre, A., Boyer-Chatenet, L. & Gautier, J. Two-step activation of ATM by DNA and the Mre11-Rad50-Nbs1 complex. *Nat Struct Mol Biol* **13**, 451-7 (2006).
91. Bakkenist, C.J. & Kastan, M.B. DNA damage activates ATM through intermolecular autophosphorylation and dimer dissociation. *Nature* **421**, 499-506. (2003).
92. Stucki, M. et al. MDC1 directly binds phosphorylated histone H2AX to regulate cellular responses to DNA double-strand breaks. *Cell* **123**, 1213-26 (2005).
93. Melander, F. et al. Phosphorylation of SDT repeats in the MDC1 N terminus triggers retention of NBS1 at the DNA damage-modified chromatin. *J Cell Biol* **181**, 213-26 (2008).
94. Wang, J., Gong, Z. & Chen, J. MDC1 collaborates with TopBP1 in DNA replication checkpoint control. *J Cell Biol* **193**, 267-73 (2011).
95. Xiao, A. et al. WSTF regulates the H2A.X DNA damage response via a novel tyrosine kinase activity. *Nature* **457**, 57-62 (2009).
96. Cook, P.J. et al. Tyrosine dephosphorylation of H2AX modulates apoptosis and survival decisions. *Nature* **458**, 591-6 (2009).
97. Iliakis, G., Wang, Y., Guan, J. & Wang, H. DNA damage checkpoint control in cells exposed to ionizing radiation. *Oncogene* **22**, 5834-47 (2003).
98. Lukas, J., Lukas, C. & Bartek, J. Mammalian cell cycle checkpoints: signalling pathways and their organization in space and time. *DNA Repair (Amst)* **3**, 997-1007 (2004).
99. Morgan, D.O. The Cell Cycle Principles of Control (New Scicence Press, London, 2007).
100. Ikura, T. et al. DNA damage-dependent acetylation and ubiquitination of H2AX enhances chromatin dynamics. *Mol Cell Biol* **27**, 7028-40 (2007).
101. Mailand, N. et al. RNF8 ubiquitylates histones at DNA double-strand breaks and promotes assembly of repair proteins. *Cell* **131**, 887-900 (2007).
102. Bekker-Jensen, S. et al. HERC2 coordinates ubiquitin-dependent assembly of DNA repair factors on damaged chromosomes. *Nat Cell Biol* **12**, 80-6; sup pp 1-12 (2010).
103. Stewart, G.S. et al. The RIDDLE syndrome protein mediates a ubiquitin-dependent signaling cascade at sites of DNA damage. *Cell* **136**, 420-34 (2009).
104. Doil, C. et al. RNF168 binds and amplifies ubiquitin conjugates on damaged chromosomes to allow accumulation of repair proteins. *Cell* **136**, 435-46 (2009).

105. Yan, J. et al. The ubiquitin-interacting motif containing protein RAP80 interacts with BRCA1 and functions in DNA damage repair response. *Cancer Res* **67**, 6647-56 (2007).
106. Wang, B. et al. Abraxas and RAP80 form a BRCA1 protein complex required for the DNA damage response. *Science* **316**, 1194-8 (2007).
107. Sobhian, B. et al. RAP80 targets BRCA1 to specific ubiquitin structures at DNA damage sites. *Science* **316**, 1198-202 (2007).
108. Galanty, Y. et al. Mammalian SUMO E3-ligases PIAS1 and PIAS4 promote responses to DNA double-strand breaks. *Nature* **462**, 935-9 (2009).
109. Morris, J.R. et al. The SUMO modification pathway is involved in the BRCA1 response to genotoxic stress. *Nature* **462**, 886-90 (2009).
110. Markova, E., Schultz, N. & Belyaev, I.Y. Kinetics and dose-response of residual 53BP1/gamma-H2AX foci: co-localization, relationship with DSB repair and clonogenic survival. *Int J Radiat Biol* **83**, 319-29 (2007).
111. Yamauchi, M. et al. Growth of persistent foci of DNA damage checkpoint factors is essential for amplification of G1 checkpoint signaling. *DNA Repair (Amst)* **7**, 405-17 (2008).
112. Yoshikawa, T., Kashino, G., Ono, K. & Watanabe, M. Phosphorylated H2AX foci in tumor cells have no correlation with their radiation sensitivities. *J Radiat Res (Tokyo)* **50**, 151-60 (2009).
113. Rodier, F. et al. Persistent DNA damage signalling triggers senescence-associated inflammatory cytokine secretion. *Nat Cell Biol* **11**, 973-9 (2009).
114. Svetlova, M.P., Solovjeva, L.V. & Tomilin, N.V. Mechanism of elimination of phosphorylated histone H2AX from chromatin after repair of DNA double-strand breaks. *Mutat Res* **685**, 54-60 (2010).
115. Kimura, H. et al. A novel histone exchange factor, protein phosphatase 2Cgamma, mediates the exchange and dephosphorylation of H2A-H2B. *J Cell Biol* **175**, 389-400 (2006).
116. Chowdhury, D. et al. gamma-H2AX dephosphorylation by protein phosphatase 2A facilitates DNA double-strand break repair. *Mol Cell* **20**, 801-9 (2005).
117. Chowdhury, D. et al. A PP4-phosphatase complex dephosphorylates gamma-H2AX generated during DNA replication. *Mol Cell* **31**, 33-46 (2008).
118. Nakada, S., Chen, G.I., Gingras, A.C. & Durocher, D. PP4 is a gamma H2AX phosphatase required for recovery from the DNA damage checkpoint. *EMBO Rep* **9**, 1019-26 (2008).
119. Douglas, P. et al. Protein phosphatase 6 interacts with the DNA-dependent protein kinase catalytic subunit and dephosphorylates gamma-H2AX. *Mol Cell Biol* **30**, 1368-81.

120. Macurek, L. et al. Wip1 phosphatase is associated with chromatin and dephosphorylates gammaH2AX to promote checkpoint inhibition. *Oncogene* **29**, 2281-91.
121. Moon, S.H., Nguyen, T.A., Darlington, Y., Lu, X. & Donehower, L.A. Dephosphorylation of gamma-H2AX by WIP1: an important homeostatic regulatory event in DNA repair and cell cycle control. *Cell Cycle* **9**, 2092-6.
122. Lavin, M.F. & Shiloh, Y. The genetic defect in ataxia-telangiectasia. *Annu Rev Immunol* **15**, 177-202 (1997).
123. Taylor, A.M. Chromosome instability syndromes. *Best Pract Res Clin Haematol* **14**, 631-44 (2001).
124. Schwarz, K. et al. RAG mutations in human B cell-negative SCID. *Science* **274**, 97-9 (1996).
125. Moshous, D. et al. Artemis, a novel DNA double-strand break repair/V(D)J recombination protein, is mutated in human severe combined immune deficiency. *Cell* **105**, 177-86 (2001).
126. Noordzij, J.G. et al. Radiosensitive SCID patients with Artemis gene mutations show a complete B-cell differentiation arrest at the pre-B-cell receptor checkpoint in bone marrow. *Blood* **101**, 1446-52 (2003).
127. Li, L. et al. A founder mutation in Artemis, an SNM1-like protein, causes SCID in Athabascan-speaking Native Americans. *J Immunol* **168**, 6323-9 (2002).
128. Kobayashi, N. et al. Novel Artemis gene mutations of radiosensitive severe combined immunodeficiency in Japanese families. *Hum Genet* **112**, 348-52 (2003).
129. Riballo, E. et al. Identification of a defect in DNA ligase IV in a radiosensitive leukaemia patient. *Curr Biol* **9**, 699-702 (1999).
130. O'Driscoll, M. et al. DNA ligase IV mutations identified in patients exhibiting developmental delay and immunodeficiency. *Mol Cell* **8**, 1175-85 (2001).
131. Buck, D. et al. Cernunnos, a novel nonhomologous end-joining factor, is mutated in human immunodeficiency with microcephaly. *Cell* **124**, 287-99 (2006).
132. Meek, K. et al. SCID in Jack Russell terriers: a new animal model of DNA-PKcs deficiency. *J Immunol* **167**, 2142-50 (2001).
133. Ruis, B.L., Fattah, K.R. & Hendrickson, E.A. The catalytic subunit of DNA-dependent protein kinase regulates proliferation, telomere length, and genomic stability in human somatic cells. *Mol Cell Biol* **28**, 6182-95 (2008).
134. Wiler, R. et al. Equine severe combined immunodeficiency: a defect in V(D)J recombination and DNA-dependent protein kinase activity. *Proc Natl Acad Sci U S A* **92**, 11485-9 (1995).
135. Blunt, T. et al. Defective DNA-dependent protein kinase activity is linked to V(D)J recombination and DNA repair defects associated with the murine scid mutation. *Cell* **80**, 813-23 (1995).

136. van der Burg, M. et al. A DNA-PKcs mutation in a radiosensitive T-B- SCID patient inhibits Artemis activation and nonhomologous end-joining. *J Clin Invest* **119**, 91-8 (2009).
137. Gu, Y. et al. Growth retardation and leaky SCID phenotype of Ku70-deficient mice. *Immunity* **7**, 653-65 (1997).
138. Zhu, C., Bogue, M.A., Lim, D.S., Hasty, P. & Roth, D.B. Ku86-deficient mice exhibit severe combined immunodeficiency and defective processing of V(D)J recombination intermediates. *Cell* **86**, 379-89 (1996).
139. Nussenzweig, A. et al. Requirement for Ku80 in growth and immunoglobulin V(D)J recombination. *Nature* **382**, 551-5 (1996).
140. Li, G., Nelsen, C. & Hendrickson, E.A. Ku86 is essential in human somatic cells. *Proc Natl Acad Sci U S A* **99**, 832-7 (2002).
141. Stewart, G.S. et al. RIDDLE immunodeficiency syndrome is linked to defects in 53BP1-mediated DNA damage signaling. *Proc Natl Acad Sci U S A* **104**, 16910-5 (2007).
142. Devgan, S.S. et al. Homozygous deficiency of ubiquitin-ligase ring-finger protein RNF168 mimics the radiosensitivity syndrome of ataxia-telangiectasia. *Cell Death Differ* **18**, 1500-6 (2011).
143. Banath, J.P. & Olive, P.L. Expression of phosphorylated histone H2AX as a surrogate of cell killing by drugs that create DNA double-strand breaks. *Cancer Res* **63**, 4347-50 (2003).
144. Muslimovic, A., Nystrom, S., Gao, Y. & Hammarsten, O. Numerical analysis of etoposide induced DNA breaks. *PLoS One* **4**, e5859 (2009).
145. Rothkamm, K. & Lobrich, M. Evidence for a lack of DNA double-strand break repair in human cells exposed to very low x-ray doses. *Proc Natl Acad Sci U S A* **100**, 5057-62 (2003).
146. Lobrich, M. et al. In vivo formation and repair of DNA double-strand breaks after computed tomography examinations. *Proc Natl Acad Sci U S A* **102**, 8984-9 (2005).
147. Beels, L., Bacher, K., De Wolf, D., Werbrouck, J. & Thierens, H. gamma-H2AX foci as a biomarker for patient X-ray exposure in pediatric cardiac catheterization: are we underestimating radiation risks? *Circulation* **120**, 1903-9 (2009).
148. Kuefner, M.A. et al. Effect of CT scan protocols on x-ray-induced DNA double-strand breaks in blood lymphocytes of patients undergoing coronary CT angiography. *Eur Radiol* **20**, 2917-24.
149. Kuefner, M.A. et al. DNA double-strand breaks and their repair in blood lymphocytes of patients undergoing angiographic procedures. *Invest Radiol* **44**, 440-6 (2009).
150. Qvarnstrom, O.F., Simonsson, M., Johansson, K.A., Nyman, J. & Turesson, I. DNA double strand break quantification in skin biopsies. *Radiother Oncol* **72**, 311-7 (2004).

151. Sak, A. et al. gamma-H2AX foci formation in peripheral blood lymphocytes of tumor patients after local radiotherapy to different sites of the body: dependence on the dose-distribution, irradiated site and time from start of treatment. *Int J Radiat Biol* **83**, 639-52 (2007).
152. Kinders, R.J. et al. Development of a validated immunofluorescence assay for gammaH2AX as a pharmacodynamic marker of topoisomerase I inhibitor activity. *Clin Cancer Res* **16**, 5447-57.
153. Wang, L.H. et al. Monitoring drug-induced gammaH2AX as a pharmacodynamic biomarker in individual circulating tumor cells. *Clin Cancer Res* **16**, 1073-84.
154. Redon, C.E. et al. The use of gamma-H2AX as a biodosimeter for total-body radiation exposure in non-human primates. *PLoS One* **5**, e15544.
155. Garty, G. et al. The RABIT: a rapid automated biodosimetry tool for radiological triage. *Health Phys* **98**, 209-17.
156. Cornelissen, B. et al. Imaging DNA damage in vivo using gammaH2AX-targeted immunoconjugates. *Cancer Res* **71**, 4539-49.
157. Porcedda, P. et al. A rapid flow cytometry test based on histone H2AX phosphorylation for the sensitive and specific diagnosis of ataxia telangiectasia. *Cytometry A* **73**, 508-16 (2008).
158. Bourton, E.C., Plowman, P.N., Smith, D., Arlett, C.F. & Parris, C.N. Prolonged expression of the gamma-H2AX DNA repair biomarker correlates with excess acute and chronic toxicity from radiotherapy treatment. *Int J Cancer*.
159. Andrievski, A. & Wilkins, R.C. The response of gamma-H2AX in human lymphocytes and lymphocytes subsets measured in whole blood cultures. *Int J Radiat Biol* **85**, 369-76 (2009).
160. Muslimovic, A., Ismail, I.H., Gao, Y. & Hammarsten, O. An optimized method for measurement of gamma-H2AX in blood mononuclear and cultured cells. *Nat Protoc* **3**, 1187-93 (2008).
161. Matsuzaki, K., Harada, A., Takeiri, A., Tanaka, K. & Mishima, M. Whole cell-ELISA to measure the gammaH2AX response of six aneugens and eight DNA-damaging chemicals. *Mutat Res* **700**, 71-9.
162. Yip, K.W. et al. A high-content screening (HCS) assay for the identification of chemical inducers of PML oncogenic domains (PODs). *J Biomol Screen* **16**, 251-8.
163. Fortune, J.M. & Osheroff, N. Topoisomerase II as a target for anticancer drugs: when enzymes stop being nice. *Prog Nucleic Acid Res Mol Biol* **64**, 221-53 (2000).
164. Johansson, P., Muslimovic, A., Hultborn, R., Fernstrom, E. & Hammarsten, O. In-solution staining and arraying method for the immunofluorescence detection of gammaH2AX foci optimized for clinical applications. *Biotechniques* **51**, 185-9 (2011).